*Progress In Electromagnetics Research B, Vol. 92, 19–45, 2021*

# Characteristics Mode Analysis: A review of Its Concepts, Recent Trends, State-of-the-Art Developments and Its Interpretation with a Fractal UWB MIMO Antenna

**Asutosh Mohanty[1, *] and Bikash R. Behera[2]**

**Abstract**—In this article, we present a compact and efficient diametrically-fed dual port fractal UWB MIMO antenna for portable handheld wireless devices. The electromagnetic behaviour on conducting body is analyzed through classical approach based characteristics mode analysis (CMA). Their intrinsic characteristics are explored on the basis of (a) modal surface current distributions, (b) narrow/broad bandwidth capability, and (c) radiation potentials. Concurrent analysis is persuaded on a diametrically-fed dual-port fed fractal conducting surface, which provides interesting facets on the combinatory effect of electromagnetic performance and physical behaviour on metallic radiator, metallic ground planes (unconnected/connected) and combination of two aforementioned metallic compact geometries. Theoretical insights are investigated for essential/non-essential modes existing in proposed geometry. The investigation through CMA also gives plethoric information on the feed location of antenna on modal surface currents and similar trends to capture its radiation potentials on the current nulls existing in the physical body. A broad classification of modes is explained, covering the CMA modal dynamics such as (a) characteristics angle (CA), (b) eigenvalues (EV), and (c) modal significance (MS). These additive parameters in general reflect the resemblance of $Q$-factor $\approx$ B.W. for narrowband/wideband traits, electrically/magnetically coupled energy behaviour, and radiative potential for far-field propagation. Thus, in a nut-shell, it can be concluded that 'CMA provides physically intuitive guidance for the analysis and designing of antenna structures'. To support the findings highlighted in this particular study, a concise review about the theory of characteristic modes and the practical examples that use such concepts are taken into consideration.

## 1. INTRODUCTION

In the era of using computational electromagnetism for full wave analysis, the concurrent research is directed towards utilizing such type of concepts, which in general helps the antenna designers in designing RF front-ends that satisfies tradeoffs from applications point of view. In such a scenario, incorporation of characteristics mode analysis (CMA) has opened new way-out for maximizing outcomes, by playing crucial role [1, 2]. The concept of CMA was originally proposed by Garbacz [3, 4], refined by Harrington and Mautz [5, 6] in terms of classical electromagnetism. The analysis of CMA produces a set of independent current patterns, i.e., modes, which naturally exist on an arbitrary structure at a given frequency. At any frequency, one can calculate infinite number of modes. Some of them might be closer to their natural resonance, and if excited, it would be able to radiate significantly. Others may be far from their natural resonance, and as a result, they will store more energy and radiate less power. Substantially, some of them might be easily excited, whereas others may not act in the same

*Received 5 February 2021, Accepted 17 March 2021, Scheduled 24 March 2021*
* Corresponding author: Asutosh Mohanty (asutoshmohanty.kiit0409@gmail.com).
[1] School of Electronics, KIIT Deemed To Be University Bhubaneswar, Odisha 751021, India. [2] Advanced RF and Microwave Lab, IIIT Bhubaneswar, Odisha 751003, India.

manner. In general, the current patterns that naturally exist on a structure are quite valuable to an antenna designer [7]. Harrington and Mautz [5] started with integral equations for the surface currents in the frequency domain. This closely ties CMA to the method of moments (MoM) [8], i.e., it works with the impedance matrix in MoM analysis. In simplified understanding, characteristic modes are the current modes that correspond to the eigenvectors of a particular weighted eigenvalue equation, involving generalized impedance matrix of the conductor. Hence, characteristic modes can be used to expand the total current on the conductor surface, which can be extended for the dielectrics [9]. In fact, it makes the utilization of characteristic modes more attractive for antenna design, which helps to obtain physical insights into antenna radiation [10, 11]. There is characteristic angle (CA) or eigenvalues (EV) associated, which provides information about mode resonances and radiating characteristics [12]. Its quantitative analysis is significantly dependent on the shape and size of the conducting object. Thus, the process of antenna designing should be performed in controlled manner, based on the needs of applications present in wireless communication platform [13–18].

Now coming to the applications point of view, portable hand-held wireless devices are of great demand for its necessity in personal digital assistants (PDAs)/personal area networks (PAN). They include smart multipurpose functionalities such as messaging, scanning, audio/video recording; personal communication services (PCS) like cellular telephones, smart phones, tablets, two-way pagers, handheld radios, bluetooth speakers, and newly introduced Alexa-enabled smart speakers. These PDAs require a multi-port assistant for smarter connectivity, which is why multi-port antennas are introduced to proliferate its data connectivity in a compact wireless integrated portable system [19–21]. Thus, multiple-input-multiple-output (MIMO) proves to be the best solution [22–28]. For portable handheld smarter devices, usually the dual/tri-port antenna systems are feasible [29, 30]. However, the real challenge from antenna designers' point of view is the requirement of multiband frequency systems, such as PDA, PCS, PAN operating at different frequency ranges. So, ultra-wideband (UWB) [31, 32] is considered as the only solution to capture all the operating associated bands in 3.1–10.6 GHz. Another

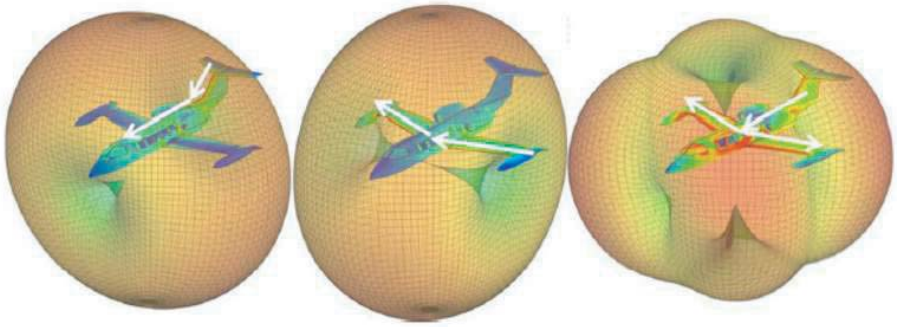

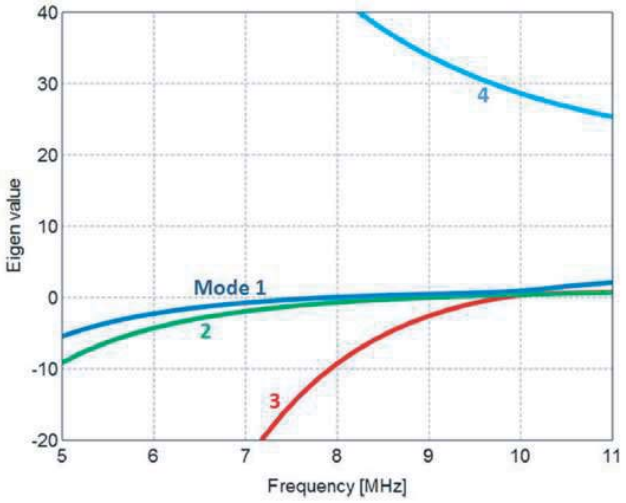


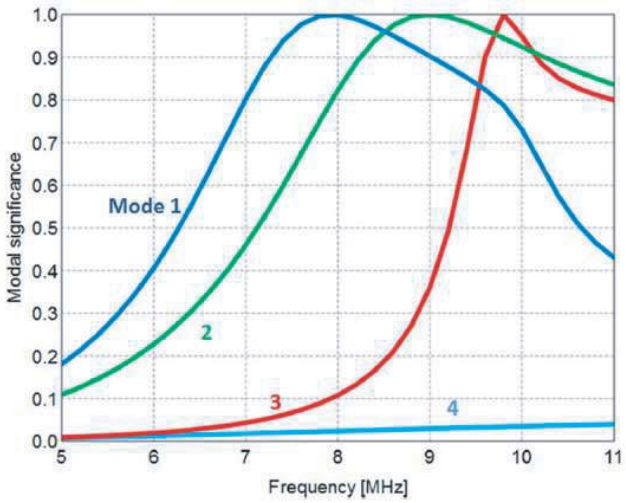

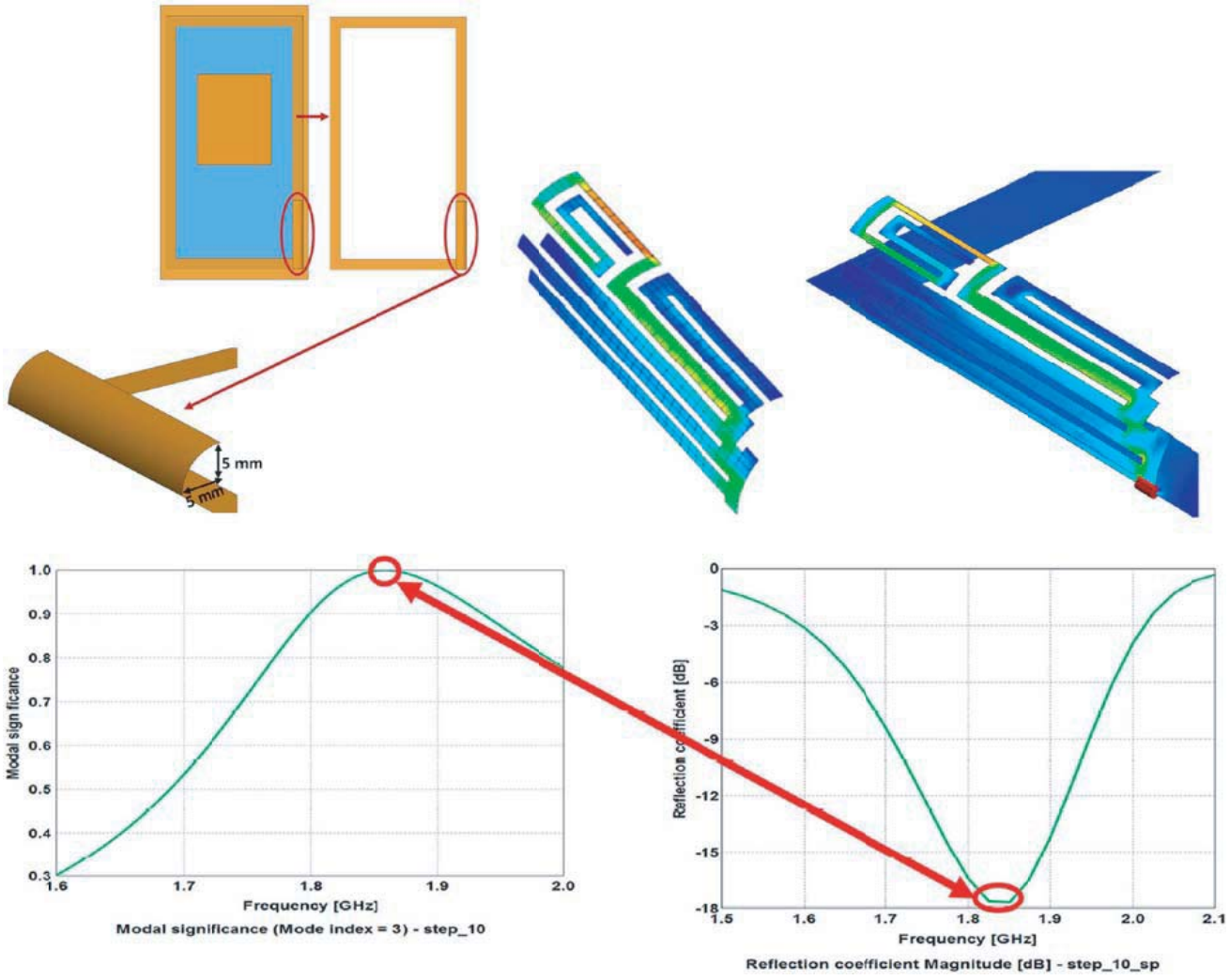


**Figure 1.** Classic examples: HF communication and LTE antenna for cell phones, where CMA is explored [1].

challenge is to fit appropriate antenna and generate multiple resonating spectrums [33–35]. Thus, the phenomenon of self-similar antenna structures commonly known as Fractals, is introduced and considered as the optimum solution, as it provides multi-resonances with wide bandwidth [36–39]. The self-similar structures are complex on design perspective, as the conducting surface has intricate geometry. So, it is difficult to predict its intrinsic physical characteristics such as feed location, surface current distributions, and radiation patterns. The aforementioned issues are resolved by an intuitive classical approach based characteristics mode analysis (CMA) [40–50], as shown in Figure 1.

Nevertheless, when the electromagnetic numerical calculation is used to determine the modal proportion, each characteristic current is discretely distributed on the structure meshes, making it difficult to determine a modal proportion using mode currents. On the other hand, far-field of each mode is contributed by the overall current of the corresponding modes. It is also proposed to use the radiation field of the corresponding mode to quantify the modal proportion. The estimation of modal proportion using only field values in a certain spatial direction helps to verify that the antenna is designed in compliance with the desired requirements from application point of view [12]. To further strengthen our study, we have proposed a compact and efficient diametrically-fed dual-port fractal UWB MIMO antenna for portable handheld wireless devices [51]. The electromagnetic behaviour on conducting body is analysed through CMA. Intrinsic characteristics are explored on the basis of (a) modal surface

current distributions, (b) narrow/broad bandwidth capability, and (c) radiation potentials. Based on our findings, it provides physically intuitive guidance for the analysis and designing of antenna structures. This research article is divided in the following manner. Section 2 gives a complete idea about the CMA approach on perfectly conducting surface. To get insights about CMA, its diversity and classification of various modes, in pursuit of the proposed antenna, is given in Section 3. Section 4 explains the phenomena of resolving a complex electromagnetic radiating structure, especially fractals through characteristic mode analysis. Certain insights are presented based on design and characterization. The concepts that we have given are experimentally validated. Conclusion is presented in Section 5, followed by future works and references in Sections 6 and 7, respectively.

## 2. CMA APPROACH ON PERFECTLY CONDUCTING SURFACE

In this section, we will try to understand the extension of characteristics mode analysis (CMA) and its metrics on analysing perfectly conducting surface. The theory of CMA states that a conducting random body supports multi-characteristics modes with orthogonal characteristics modal currents ($J_n$) & weighted eigenvalues ($\lambda_n$):

$$X(J_n) = \lambda_n R(J_n) \tag{1}$$

where $[X, R]$ are considered as the imaginary and real parts of impedance operator $Z(J_n)$.

$$Z(J_n) = R(J_n) + jX(J_n) \tag{2}$$

Similarly, the total modal currents $J_{Total}$, which exists on the surface, is considered as a superposition of $n$ number of orthogonal modal currents $J_n$. It is usually represented as:

$$J_{Total} = \sum \alpha_n J_n \tag{3}$$

where $\alpha_n$ is considered as modal weighting coefficient (MWC). Understanding of MWC is quite important, because after the analysis of current distribution of the first few characteristic modes with smaller eigenvalues, the mode selection and combination are carried out with the desired antenna radiation field requirements. In that case, it is considered as an important guiding parameter for the antenna design to determine the appropriate feed point and feed structure. To gain deeper insights about such analysis, we must understand the relationship between characteristics modes and energy [52–56]. The energy that is stored in the form of reactive power ($P_X$) & radiated power ($P_R$) gives the eigenvalues ($\lambda_n$). Mathematically, it can be expressed as:

$$\lambda_n = \frac{P_X}{R_X} = \frac{\text{Reactive Power}}{\text{Radiated Power}} \tag{4}$$

Similarly, the orthogonality property of characteristics modes is interpreted:

$$\frac{1}{2}\langle J_m^*, R(J_n)\rangle = \delta_{mn} \tag{5}$$

$$\frac{1}{2}\langle J_m^*, X(J_n)\rangle = \lambda_n \delta_{mn} \tag{6}$$

$$\frac{1}{2}\langle J_m^*, Z(J_n)\rangle = (1 + j\lambda_n)\delta_{mn} \tag{7}$$

where $*$ is the conjugate operator, and $\delta_{mn}$ is the delta function. Depending upon such orthogonality property, the modal significance (MS) [56] can be computed [based on the weighted eigenvalues ($\lambda_n$)]. It can be elaborated:

$$MS = \left|\frac{1}{1 + j\lambda_n}\right| \tag{8}$$

The evaluation of characteristic angle (CA) is equally important to that of modal significance (MS). It is also based on the weighted eigenvalues ($\lambda_n$) and expressed as:

$$\phi_n = 180^\circ \left[1 - \frac{1}{\prod}\text{arc}(\tan(\lambda_n))\right] \tag{9}$$

In addition, the MWC analysis has utilized the orthogonality of the characteristic current wave mode, and each mode radiation power is first normalized to the unit value. On the other hand, the reactive power is proportional to the eigenvalue magnitude. The amplitude of a characteristic current is related to the radiation efficiency of the corresponding mode, i.e., its eigenvalue magnitude requires large mode currents to reach the same radiation power level as lower-order modes. Each characteristic mode current of the antenna structure produces a pattern of the far-field. Therefore, the corresponding modal proportion of the antenna can be verified by the proportion of the radiated field. For specific calculation, maximum radiation direction of the main mode/total far-field electric field is obtained by the full-wave method through CMA [8, 9]. Table 1 and Table 2 present the modal dynamics (a) characteristics angle, (b) modal nature, (c) modal significance, and (d) modal stored energy. In the next section, a complete classification of the family of CMA diversity (i.e., modes) is presented. To the best of the authors' knowledge, it is the first time that such type of insights is given for CMA, as shown in Figure 2.

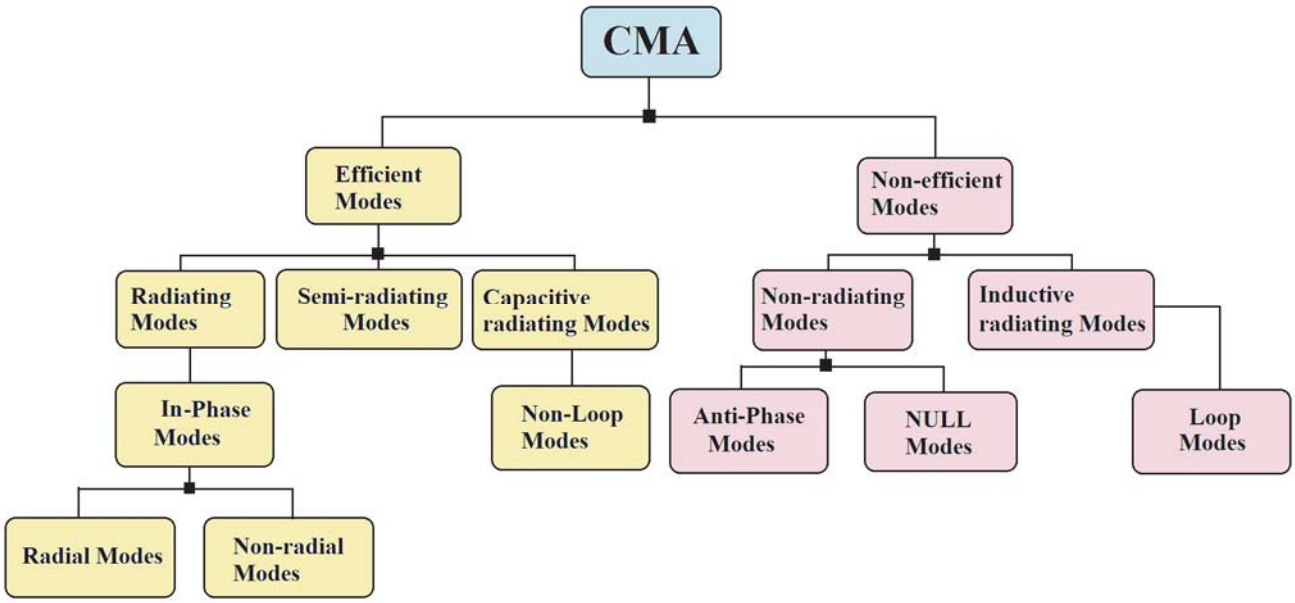


**Figure 2.** An overview of CMA diversity and its classification.

**Table 1.** Dynamics of characteristics angle (CA) as an evaluation metrics of CMA.

| **Characteristic Angle ($\phi_n$)** | **Modal Nature** |
|---|---|
| $90° < \phi_n < 180°$ | The generated modes at its operating bands are inductive in nature |
| $\phi_n = 180°$ | The generated modes at its operating bands is at resonance condition |
| $180° < \phi_n < 270°$ | The generated modes at its operating bands are capacitive in nature |

## 3. CMA DIVERSITY AND CLASSIFICATION

For the ease of antenna design and analysis on intrinsic electromagnetic behaviour, we provide CMA diversity in the broad classification of different existing modes in a conducting element, which is shown in Figure 2. In a conducting element, there exit different types of modes, when it is subjected to the supplementary excitation source. The electrons in the conducting body generate different paths directly proportional to the amount of energy supplied by the external source. Thereby, more energy leads to

**Table 2.** Dynamics of eigenvalues (EV), modal significance (MS) and modal stored energy as an evaluation metrics of CMA.

| **Eigen Value** ($\lambda_n$) | **Modal Stored Energy** | **Modal Significance (MS)** |
|---|---|---|
| $\lambda_n < 0$ | The modal stored energy is electric/capacitive energy | MS $\approx 1$ |
| $\lambda_n = 0$ | The modal stored energy is at resonance condition | MS $= 1$ |
| $\lambda_n > 0$ | The modal stored energy is magnetic/inductive energy | MS $< 1$ |

the excitation of higher modes. However, there exist some modes which participate in the covalent bonding of ions in a conductor (Hypothetical assumptions), and they are called as efficient modes, which significantly contribute in radiation mechanism. Still there exist some modes, which result in the cancellation of other significant modes due to phase reversal and looping of higher excited modes and nullify magnitudes of significant modes, along with non-significant modes. These modes do not participate in the radiating mechanism which are called as non-efficient modes. Now coming to the classification, the efficient modes are classified in their magnitude of high radiative strengths as:

1. Radiating Modes: These modes are known to have stronger magnitudes of current density, which strongly participate in other significant modes. They are potentially excited at the higher order modes, and they can be further classified as:

- In-Phase Modes: These modes have equal magnitude and phase, which align themselves additively in a perfect conducting body. Keeping with the initial conditions of magnitude and phase alignment, they are separated into:
  - Radial Modes: These modes have the same phase with equal magnitudes.
  - Non-Radial Modes: These modes have the same phase with unequal magnitudes.

2. Semi-Radiating Modes: These modes have moderately aligned equal &/or non-equal magnitude of current density.

3. Capacitive Radiating Modes: These modes have dominant stored electric field energy, which is capacitive in nature. This mode is also called as Non-Loop Modes.

- Non-Loop Modes: Due to dominant stored capacitive energy, the magnitude of electric fields is aligned radially without any loops and hence, contributes in the resonance condition.

The non-efficient modes are classified in their magnitude of low relative strengths on current density:

- Non-Radiating Modes: These modes do not participate in the radiation mechanism, because of the low magnitude of current density, non-linearity in magnitudes, and unequal phase distributions observed in the conducting element. These modes require an external source. It can be divided as:
  - Anti-Phase Modes: The modes have unequal mode distributions, and the magnitudes of modes get cancelled, due to their equal magnitude with unequal phases.
  - NULL Modes: These modes have zero magnitude of field distributions and are inherently cancelled due to non-linearity and anti-phase magnitudes.
- Inductive Radiating Modes: Due to the dominant stored inductive energy, the magnitude of magnetic fields forms a magnetic current loop. The formation of circulating loops does not contribute to resonance, and henceforth, these modes are usually not considered as significant modes. It is even divided into:
  - Loop Modes: The inductive magnetic fields generate circulating magnetic currents, hence they are termed as Loop Modes. Due to their generic characteristics, these modes are not considered to be suitable for resonance conditions.

In the next section, the classical based characteristics mode analysis (CMA) is utilized for resolving at various upfronts. Prior to simulation, the characterization of proposed fractal UWB MIMO antenna is highlighted [51].

## 4. RESOLVING A COMPLEX ELECTROMAGNETIC RADIATING STRUCTURE THROUGH CHARACTERISTIC MODE ANALYSIS

The complex electromagnetic radiating structures can be resolved through CMA aiming for (a) appropriate feeding locations, (b) bandwidth capabilities, and (c) radiation potentials. In this section, the CMA analysis is implemented on a proposed perfectly metallic conducting body (2-port fractal UWB MIMO antenna) with the help of CST microwave studio. The insights are dependent on (a) analyse surface current modal distributions, (b) determining appropriate feeding location in metallic conducting body, (c) evaluation of modal dynamics, and (d) investigating radiative mechanism. This study is based on the analysis of (a) fractal conducting element without feed, (b) fractal conducting element with feed, (c) split ground conducting element, (d) connected ground conducting element, and (e) diametrically-fed dual port conducting element [51], shown in Figures 3–8.

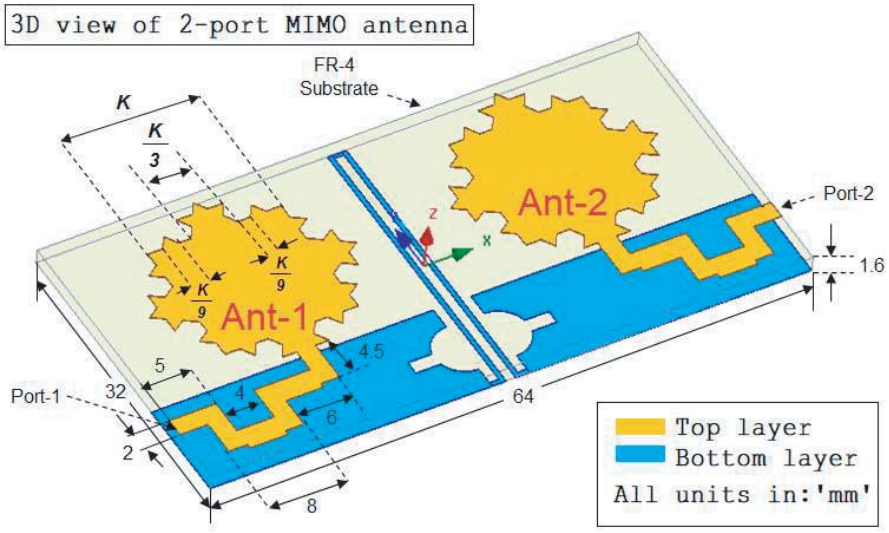


**Figure 3.** Schematic configuration of the proposed diametrically-fed dual port fractal UWB MIMO antenna.

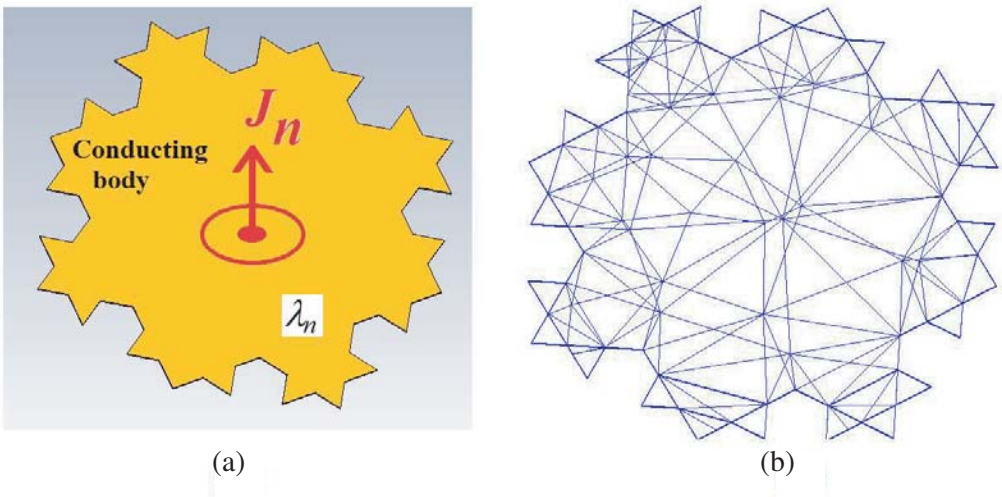


**Figure 4.** Fractal conducting element without feed, (a) perfect conducting body and (b) mesh decomposition of perfect conducting body into fine discretised characteristics modes.

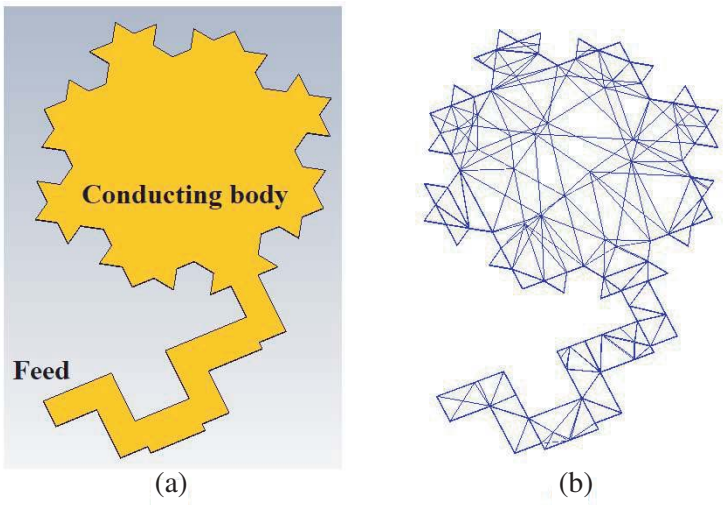


**Figure 5.** Fractal conducting element with feed, (a) perfect conducting body and (b) mesh decomposition of perfect conducting body into fine discretised characteristics modes.

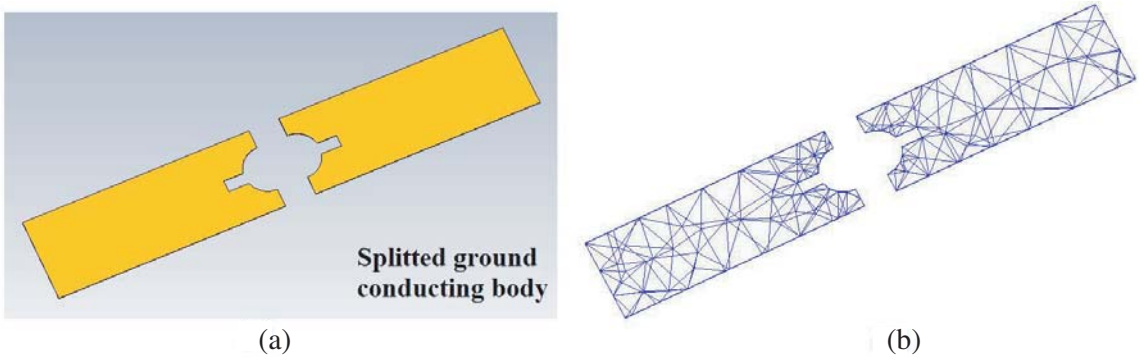


**Figure 6.** Split ground conducting element, (a) perfect conducting body and (b) mesh decomposition of perfect conducting body into fine discretised characteristics modes.

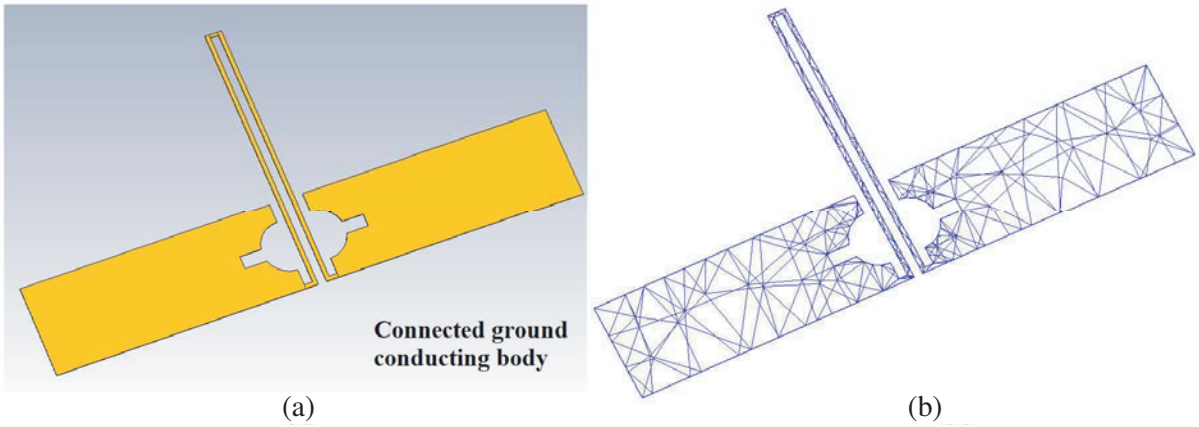


**Figure 7.** Connected ground conducting element, (a) perfect conducting body and (b) mesh decomposition of perfect conducting body into fine discretised characteristics modes.

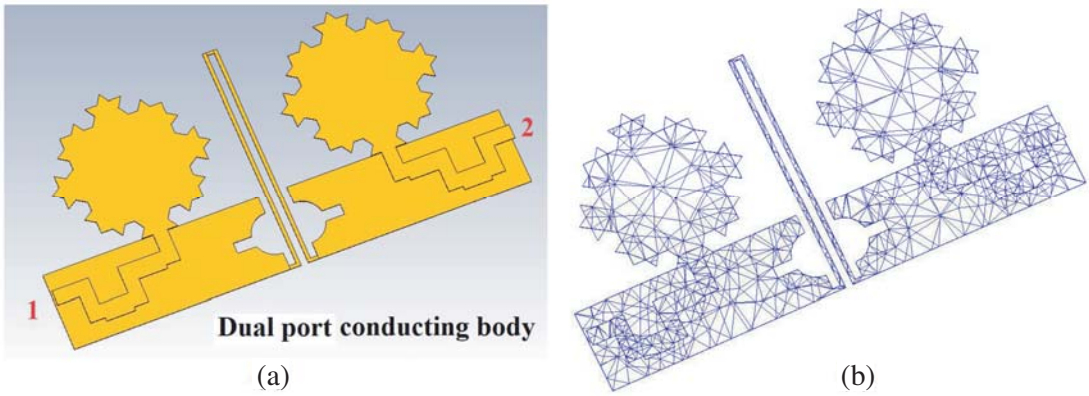


**Figure 8.** Diametrically-fed 2-port conducting element (proposed radiator), (a) perfect conducting body and (b) mesh decomposition of perfect conducting body into fine discretised characteristics modes.

### 4.1. Analysis of Fractal Conducting Element without Feed

Figure 4(a) shows the initial investigation of a perfect conducting element without feed, and Figure 4(b) shows its mesh decomposition. Modal surface current distributions are shown in Figure 9 at discrete frequencies. For all, the modal currents are strongly concentrated at vertices of fractal element. At 3 GHz, the currents are horizontally polarized in $\pm X$-direction, which are radiating in-phase modes. Figure 10 shows the modal analysis at different modes. It is observed that mode-1 is an efficient capacitive mode ($180^\circ < \phi_n < 270^\circ$) in comparison to mode-2 as inductively excited ($90^\circ < \phi_n < 180^\circ$). The eigenvalue for mode-1 is $\lambda_n < 0$ and has dominated stored electric energy while for mode-2 is $\lambda_n > 0$ has dominated stored magnetic energy. The MS converges to unity for mode-1 and shows wideband capability with low $Q$-factor, and in mode-2, it fails to attain maximum magnitude. So, mode-1 is the

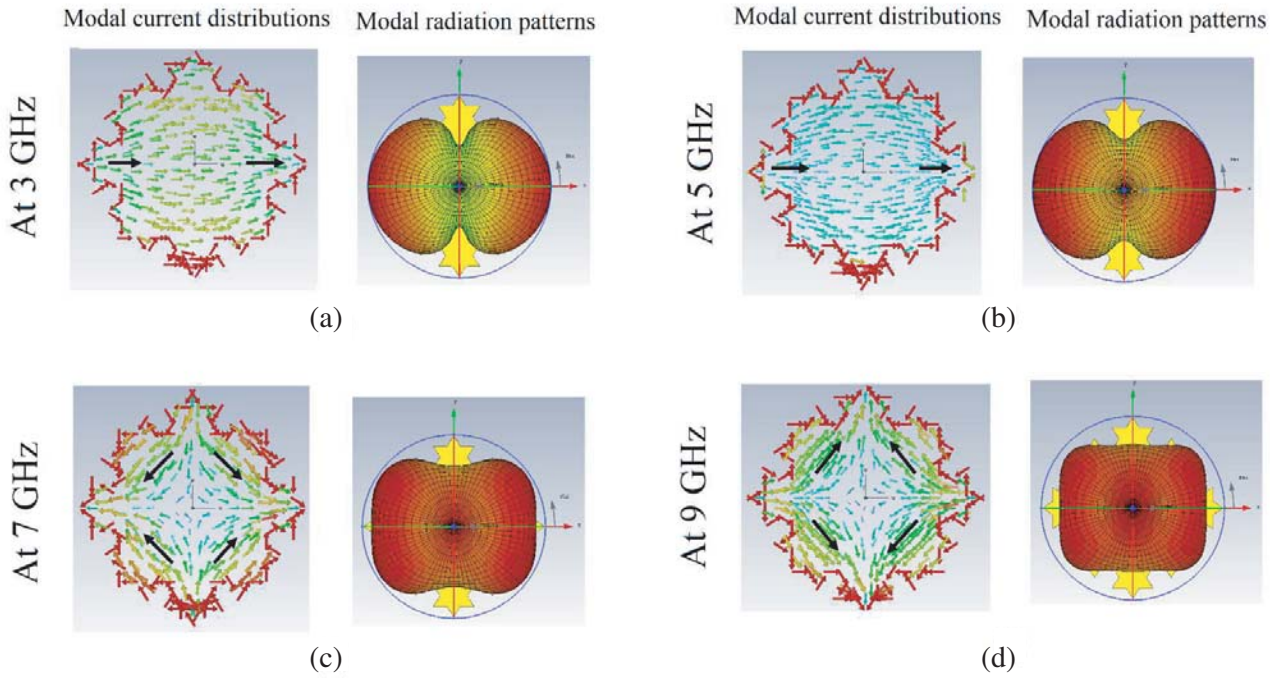


**Figure 9.** Modal current distributions and its corresponding radiation patterns at discrete frequencies.

significant mode. At 5 GHz, both mode-1 and mode-2 shown in Figure 11 act as the significant modes, in which they are horizontally polarized in $\pm X$-direction. At 7 GHz, mode-1 is considered as significant mode in comparison to mode-2 shown in Figure 12. Surface currents are $\pm 45°$ quasi-polarized. At 9 GHz, modes show wideband traits and are $\pm 45°$ quasi-polarized, since they reach maximum MS. In Figure 13, conducting body has higher order excited modes and categorized as efficient semi-radiating modes.

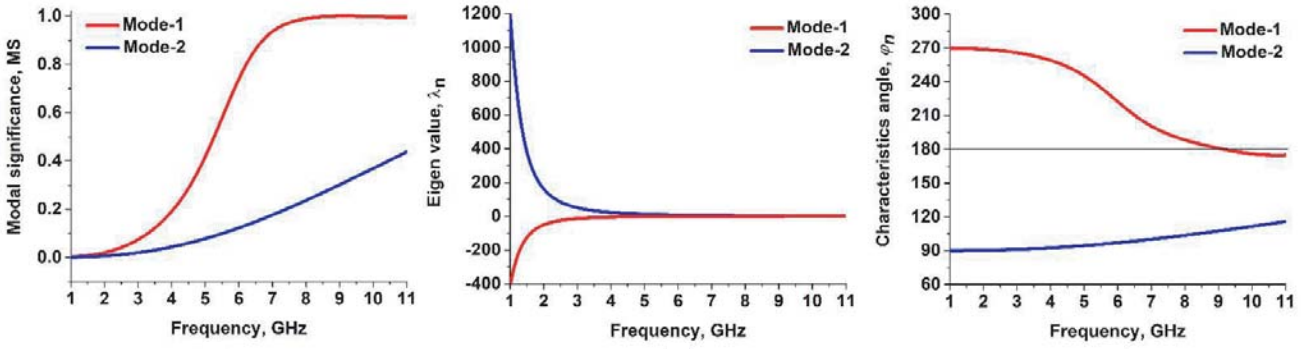


**Figure 10.** Modal analysis at 3 GHz for (a) MS, (b) $\lambda_n$ and (c) $\phi_n$.

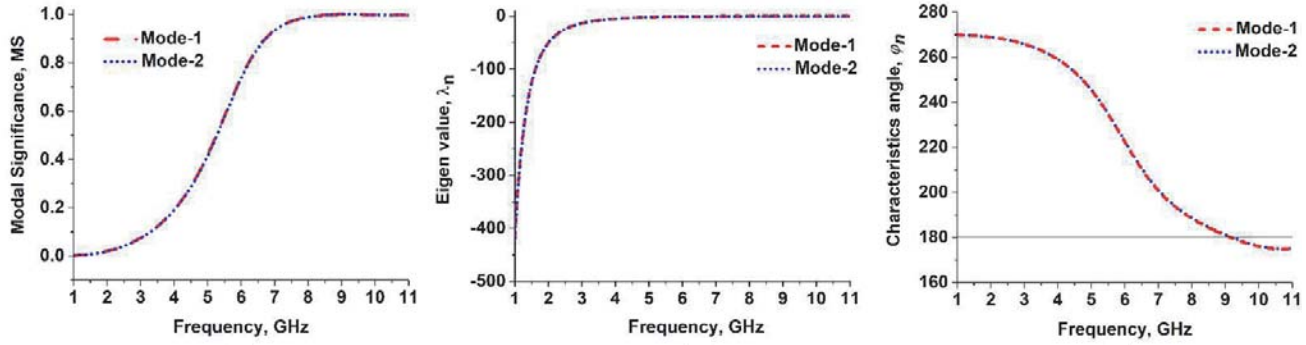


**Figure 11.** Modal analysis at 5 GHz for (a) MS, (b) Eigen Value $\lambda_n$ and (c) $\phi_n$.

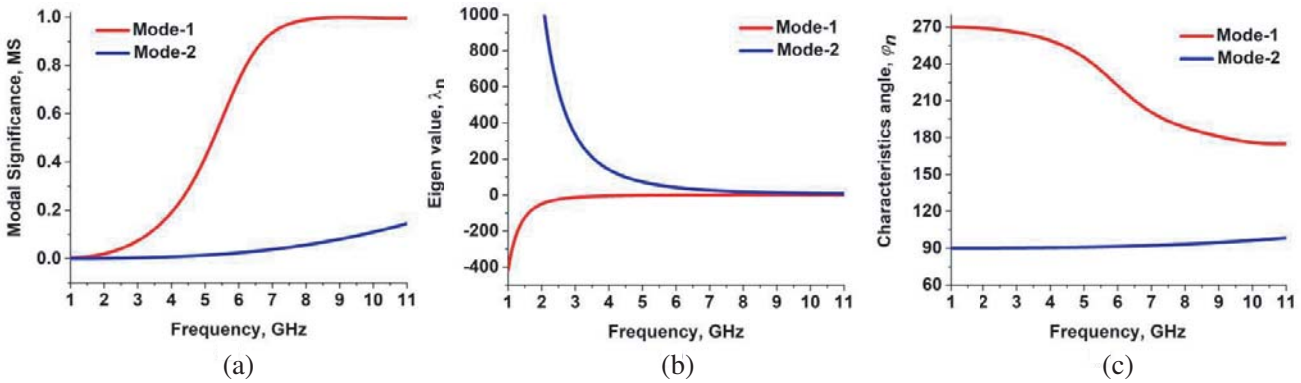


**Figure 12.** Modal analysis at 7 GHz for (a) MS, (b) $\lambda_n$ and (c) $\phi_n$.

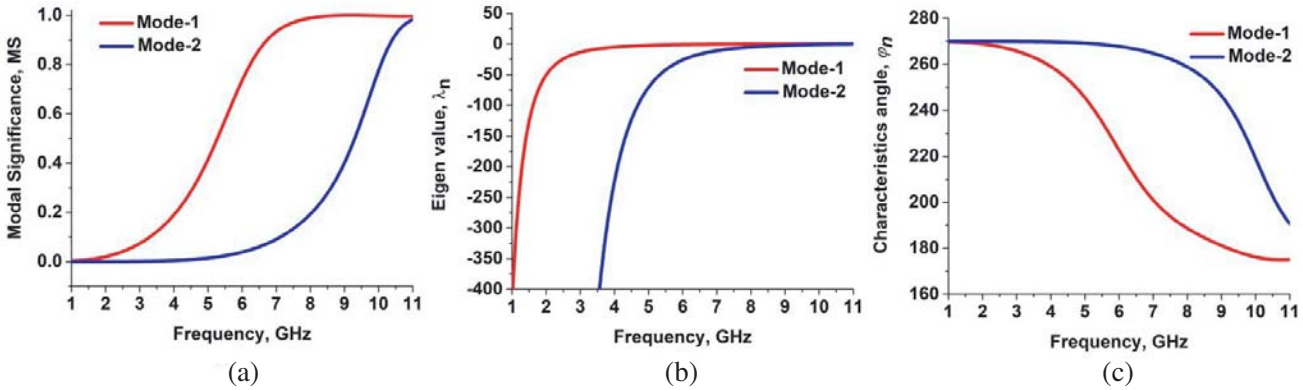


**Figure 13.** Modal analysis at 9 GHz for (a) MS, (b) $\lambda_n$ and (c) $\phi_n$.

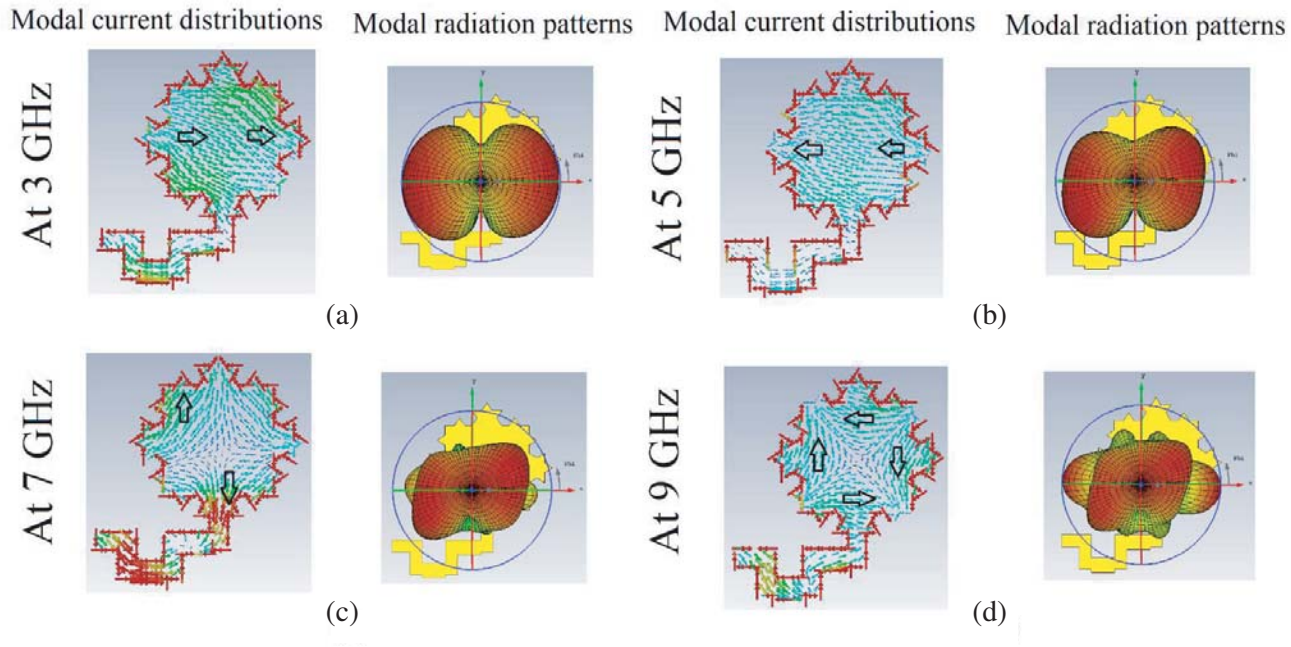


**Figure 14.** Modal current distributions and its corresponding radiation patterns at discrete frequencies.

### 4.2. Analysis of Fractal Conducting Element with Feed

Figure 5(a) shows the perfect conducting element with feed, and Figure 5(b) shows its mesh decomposition. It is observed from Figure 14 that the behaviours of radiation patterns are almost the same at 3 GHz, 5 GHz and 7 GHz, 9 GHz, respectively. Hence, for brevity we consider the lower and upper bound frequencies (3 GHz and 9 GHz) for the evaluation of modal dynamics. At 3 GHz, the surface current distributions resemble horizontally polarized patterns in $\pm X$-direction. Here, the magnitude of currents are basically in-phase radiative modes, which are aligned in a single direction. From Figure 15, it is observed that the MS has a sharper $Q$-factor with narrow bandwidth for mode-1, and for mode-2, it fails to attain maximum MS. Similarly, $\lambda_n < 0$ is capacitive in nature for mode-1 and inductive in nature $\lambda_n > 0$ for mode-2. As a result, mode-1 is considered to be significant mode, and mode-2 is also considered as non-significant mode. Even CA shows sharper response at 3 GHz, at 9 GHz, the distribution of current has quasi-directionality, which is semi-radiating with quasi-radial modes, and the MS shows a wideband response for mode-1, which can be seen in Figure 16. It is inferred

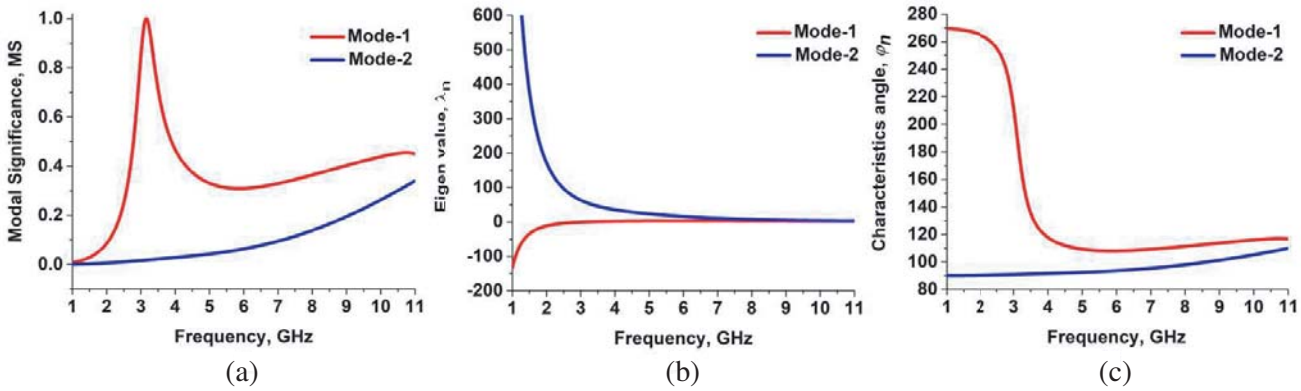


**Figure 15.** Modal analysis at 3 GHz for (a) MS, (b) $\lambda_n$ and (c) $\phi_n$.

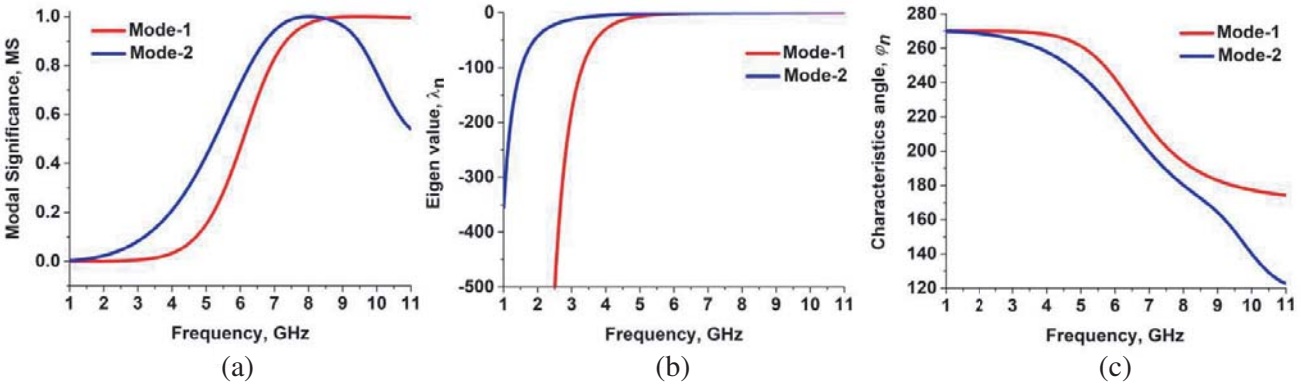


**Figure 16.** Modal analysis at 9 GHz for (a) MS, (b) $\lambda_n$ and (c) $\phi_n$.

that modal behaviour is purely dominated by stored capacitive energy ($180° < \phi_n < 270°$). Both the mode-1 and mode-2 are considered as significant modes. Due to the presence of significant modes, the proposed geometry exhibits better performance than previous counterpart. In this step, the analysis of fractal radiating element is completed. Next, we are going to show some modal dynamics about the ground (unconnected/connected).

### 4.3. Analysis of Split Ground Conducting Element

Figure 6(a) highlights split ground conducting body, and its mesh decomposition is shown in Figure 6(b). Figure 17 shows the modal surface current distributions of split ground conducting element with radiation patterns for discrete frequencies such as 3 GHz, 5 GHz, 7 GHz, and 9 GHz, respectively. Since the grounds are split/unconnected, patterns are identified through radiation NULLS. At 3 GHz, NULL currents do exist, which resides at the center. So, the radiation NULLS are observed at the center of split conducting body and can be seen in Figure 17. The maximum modal currents are denser in the center part of each split conducting body, which is polarized in $\pm X$-direction. The MS for mode-1 has wideband response compared to mode-2 as observed from Figure 18. Thus, mode-1 completely dominates mode-2. At 5 GHz, the current NULLS move away from center in either direction. Henceforth, the radiation is quite densely polarized at center. Here, both modes [mode-1 and mode-2] show stronger MS convergence due to dominant stored electric energy $\lambda_n < 0$ observed from Figure 19. So, mode-1 and mode-2 are considered the efficient anti-phase modes. At 7 GHz, the current NULLS produce two minima at each of the split conducting elements, and denser current resides in between them. As a consequence, quasi-directional radiative patterns are produced and shown in Figure 20. Here, mode-1 dominates mode-2. Thus, mode-1 is taken as a significant radiating mode observed from Figure 21. At 9 GHz, the current

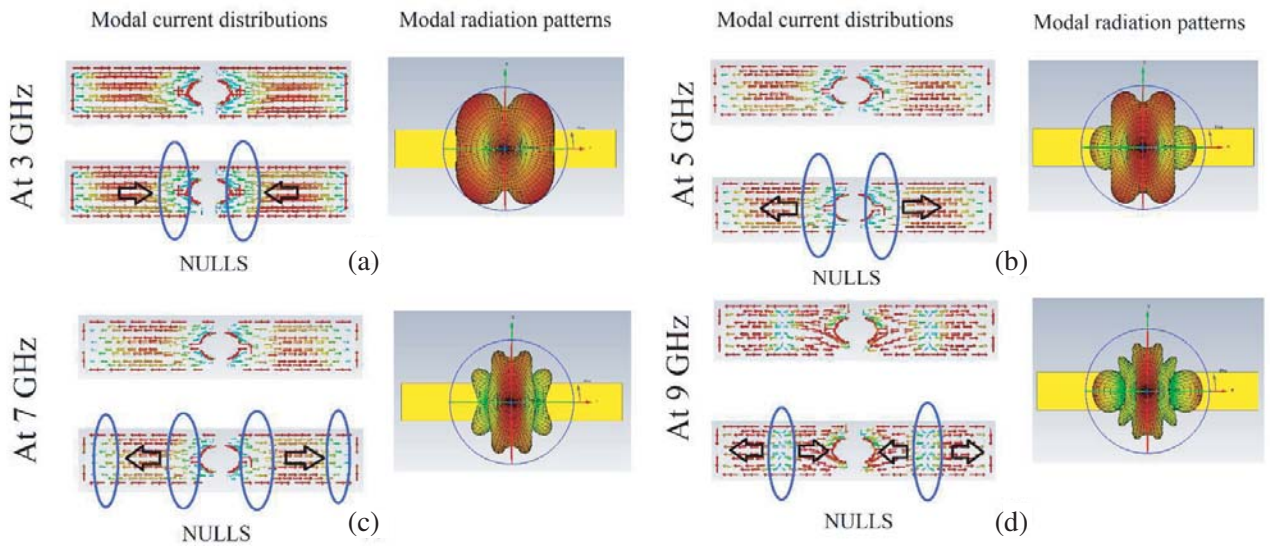


**Figure 17.** Modal current distributions and its corresponding radiation patterns at discrete frequencies.

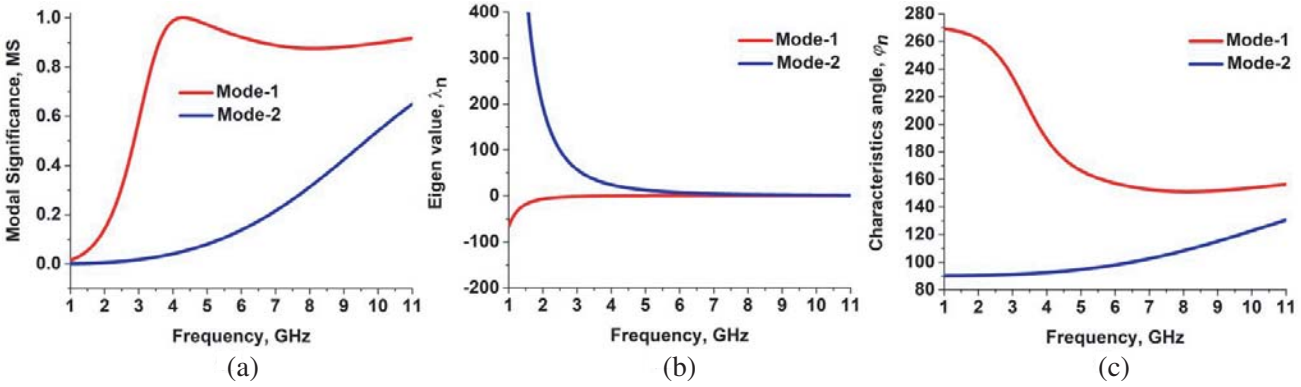


**Figure 18.** Modal analysis at 3 GHz for (a) MS, (b) $\lambda_n$ and (c) $\phi_n$.

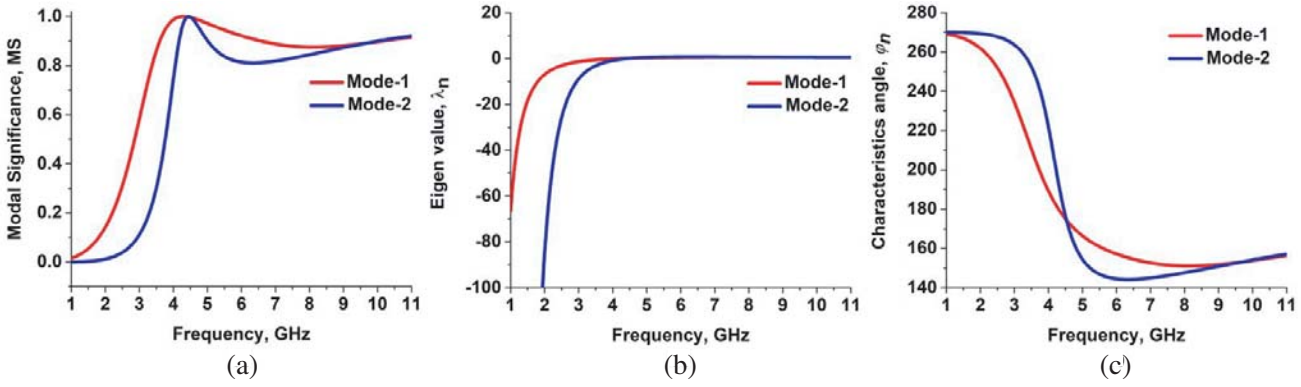


**Figure 19.** Modal analysis at 5 GHz for (a) MS, (b) $\lambda_n$ and (c) $\phi_n$.

NULLS are often suppressed by the denser currents at the ending perimeter of split elements and often radiate in either direction; as a result, quasi-directional NULLS are compressed, and broader side-lobe beams are formed. Similarly, in Figure 21, mode-1 and mode-2 show stronger MS convergence, due to the dominant capacitive energy. That is why they are considered as efficient degenerate modes.

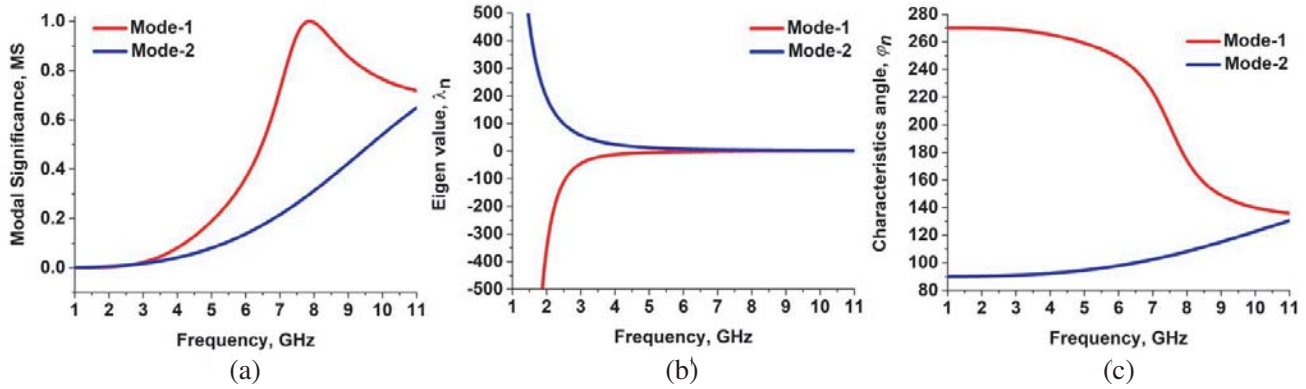


**Figure 20.** Modal analysis at 7 GHz for (a) MS, (b) $\lambda_n$ and (c) $\phi_n$.

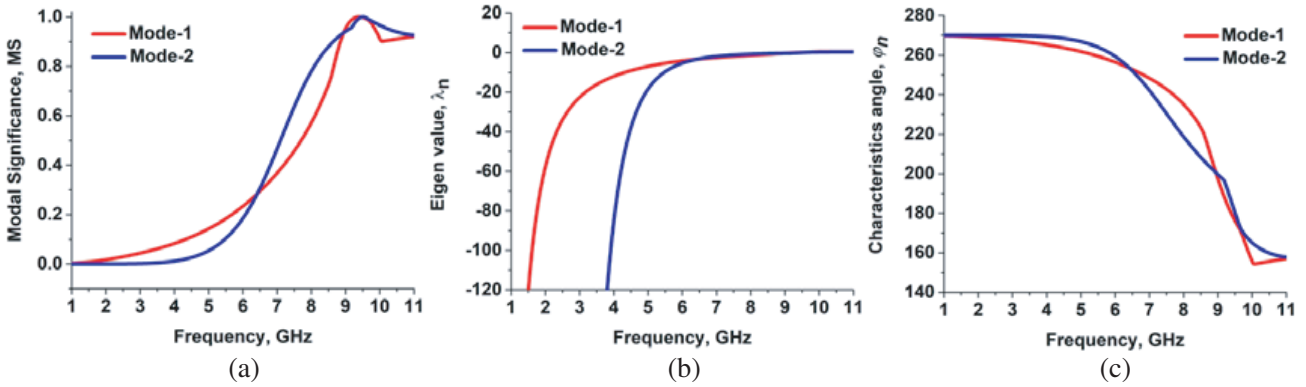


**Figure 21.** Modal analysis at 9 GHz for (a) MS, (b) $\lambda_n$ and (c) $\phi_n$.

The presence of efficient degenerate modes in the proposed geometry is expected to highlight better performance. However from the MIMO antenna design's point of view, connected ground plane would be more desirable and would be intricate effective attributes, by considering the tradeoffs [51].

### 4.4. Analysis of Connected Ground Conducting Element

Figure 7(a) shows that split ground element is connected by thin neutralization lines, and its mesh decomposition is shown in Figure 7(b). By introducing thin neutralization lines, modal current changes position and magnitude, of NULLS. At 3 GHz, NULLS at center are suppressed due to dense currents in neutralization lines. The dense modal currents have same magnitude, but oppositely directed and radiative patterns are polarized in $\pm X$-directions shown in Figure 22. These neutralization lines are also helpful in improving impedance matching in the entire operating bands. Coming to the modal dynamics, MS response has a sharp $Q$-factor with lower bandwidth for mode-1, observed from Figure 23. It is dominated by stored electric energy since $\lambda_n < 0$. The CA is capacitive for mode-1, whereas CA for mode-2 is $90^\circ < \phi_n < 180^\circ$; as a result, mode-1 is treated as the significant semi-radiating anti-phase mode. At 5 GHz, modal currents are denser at the end with two NULLS near the center, and lobes are produced in opposite directions, which can be seen in Figure 23. The modal currents of neutralization lines are concentrated at center. For mode-1, the MS has wideband response with dominating electric energy, and it is treated as capacitive radiating modes, shown in Figure 24. It shows greater magnitude than the convergent modal currents with NULLS near the center. The eigenvalues for mode-1 and mode-2 have $\lambda_n > 0$ which confirms dominated stored magnetic current loops. It is not suitable for radiation mechanism although CA has values lying in between $90^\circ < \phi_n < 180^\circ$ considered to be the non-efficient inductive radiating modes, shown in Figure 25. At 9 GHz, the modal currents have phase reversals with unequal magnitudes and produce NULLS with less dense modal currents resides

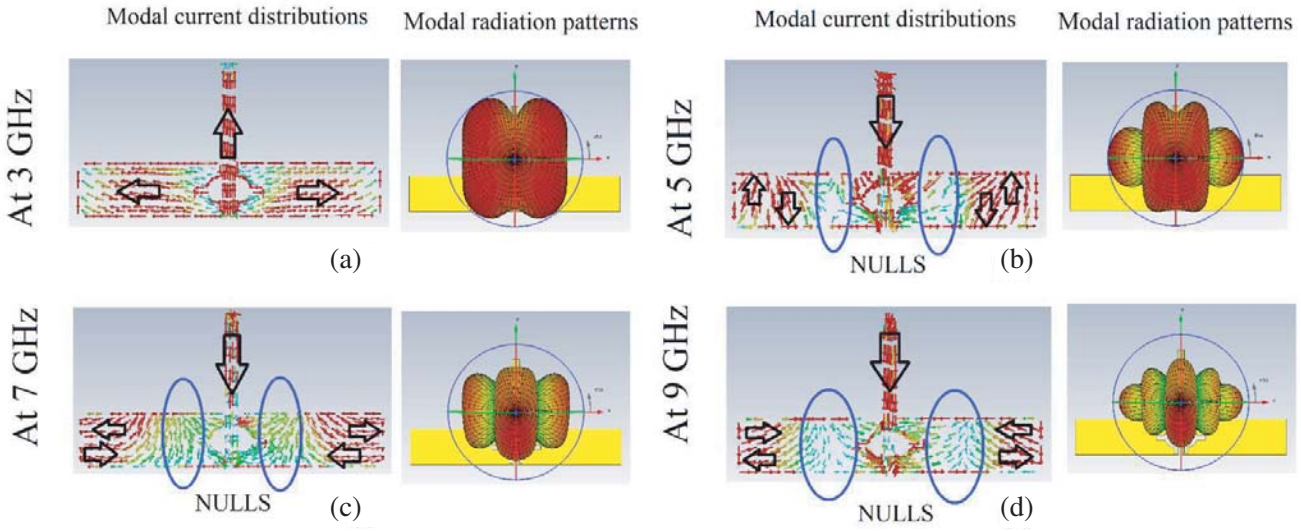


**Figure 22.** Modal current distributions and its corresponding radiation patterns at discrete frequencies.

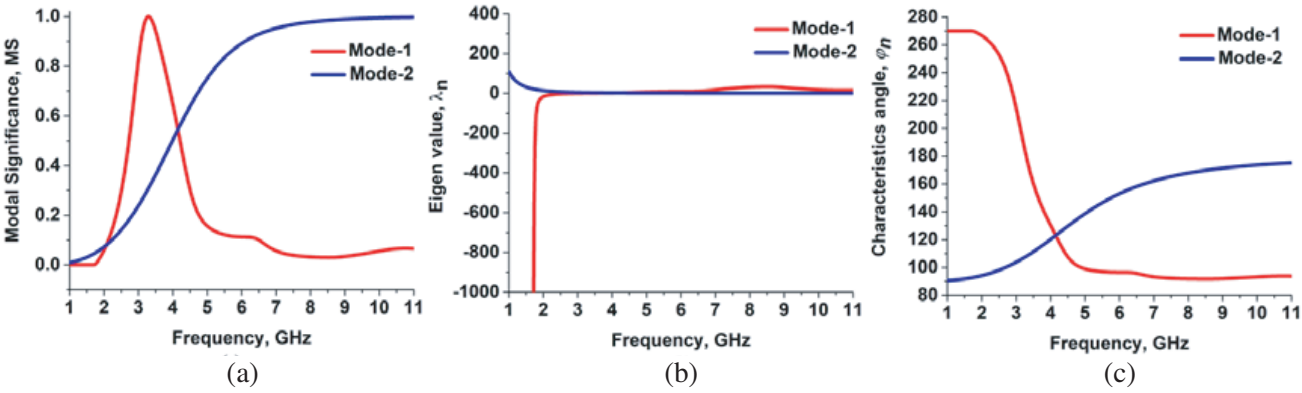


**Figure 23.** Modal analysis at 3 GHz for (a) MS, (b) $\lambda_n$ and (c) $\phi_n$.

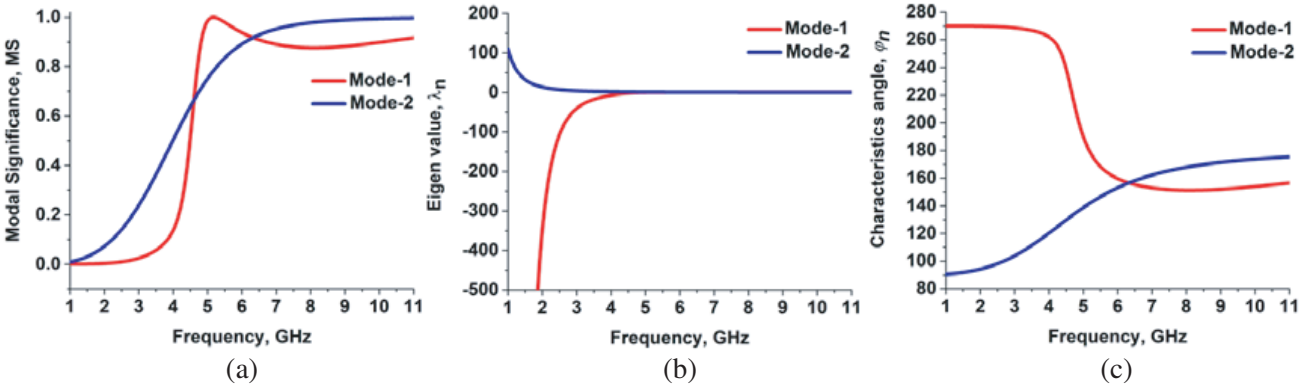


**Figure 24.** Modal analysis at 5 GHz for (a) MS, (b) $\lambda_n$ and (c) $\phi_n$.

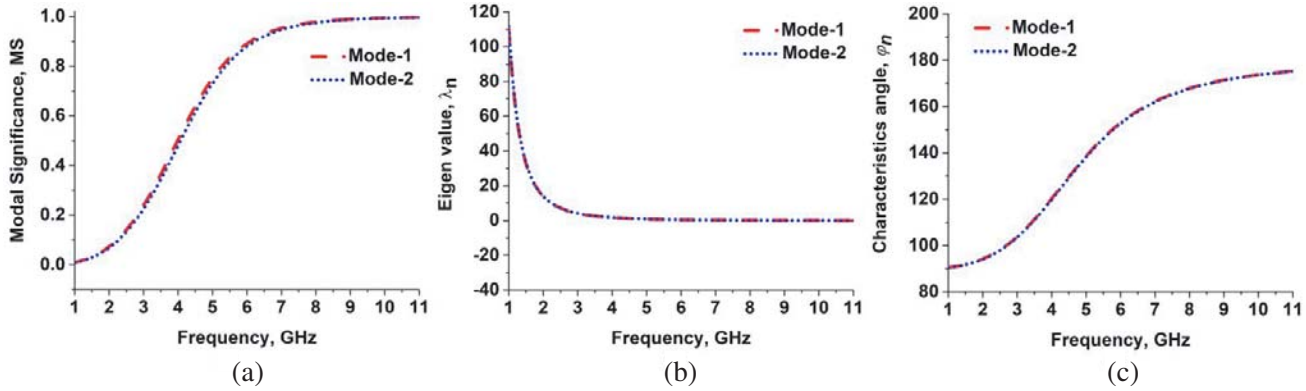


**Figure 25.** Modal analysis at 7 GHz for (a) MS, (b) $\lambda_n$ and (c) $\phi_n$.

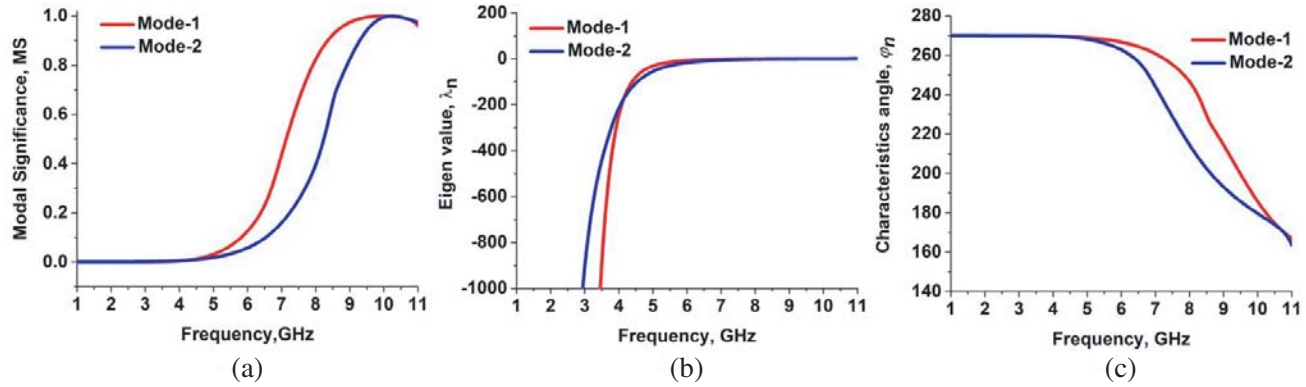


**Figure 26.** Modal analysis at 9 GHz for (a) MS, (b) $\lambda_n$ and (c) $\phi_n$.

at intermediate lobe formations, which in turn pushes the dense currents to coagulate at the conductor endings. Figure 26 highlights that the MS response for mode-1 and mode-2 shows narrow bandwidth capability, and it also suggests that both the modes are dominated by capacitive stored energy. Due to such geometrical intuition, the proposed geometry is able to exhibit desired characteristics.

### 4.5. Analysis of Diametrically-Fed Dual Port Conducting Element

Figures 8(a) and (b) show the dual-port conducting body with meshed contour. The modal current distributions are presented in Figure 27, along with its corresponding radiative patterns in Figure 28. The proposed antenna consists of a dual-port network. One port is excited, and the other port is matched terminated. Then their patterns are combined to observe the radiative potentials, shown in Figure 28 at discrete frequencies [3 GHz, 5 GHz, 7 GHz and 9 GHz]. At 3 GHz, port-1 radiates in $+X$-direction, and port-2 radiates in $-X$-direction. The radiative patterns are combined to linearly polarize in $\pm Y$-direction. At 5 GHz, port-1/port-2 radiates in $\pm X$-direction, and their patterns are combined to polarize omni-directionally. Modal currents in the proposed radiating element moves in anticlockwise directions, giving a sense of omni-directionality. At 7 GHz, radiative magnitudes have dense intensity at center and polarized in $\pm X$-directions with intermediate NULLS. When the patterns are combined, these NULLS are suppressed by dense magnitudes of side lobes, resulting in bi-directional radiative patterns. At 9 GHz, the magnitudes of mainlobes are high and polarized in $\pm X$-directions, where side lobes have lower radiation strength. When the patterns are combined, the conducting body witnesses higher excited modes, which in turn radiates linearly polarized broader lobe magnitude in $\pm X$-directions. The modal dynamics of dual-port conducting body is characterized in terms of modal performances at discrete frequency sweeps in Tables 3–6. The modal characteristics involving MS, EV,

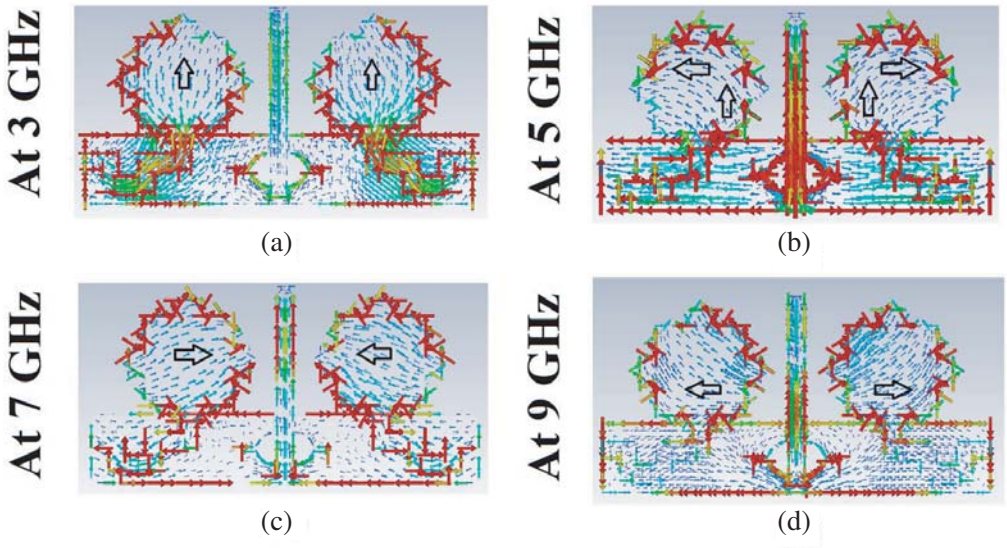


**Figure 27.** Modal current distributions at discrete frequencies.

and CA are illustrated at discretised frequency sweeps. From the observations, clear insight is given about the bandwidth capabilities confirming that modes are quite significant and support resonating conditions. It is also observed that the stored electric energy has dominating effect, and its validations are supported with modal current distributions. Figure 29 shows the modal significance (MS) for desired operating bands. Figure 30 shows the eigenvalues (EV), which confirms capacitive stored energy, and Figure 31 shows the resonating characteristics angles (CA) of the proposed fractal UWB MIMO antenna.

**Table 3.** A study of the dynamics of modal analysis at 3 GHz for diametrically-fed dual port conducting body.

| Modal Dynamics | Modal Characteristics | Modal Inference |
|---|---|---|
| MS | Sharp $Q$-Factor | Lower Bandwidth Potential |
| EV | $\lambda_n < 0$ | Capacitive Nature |
| CA | $\phi_n = 180°$ | At Resonance Condition |

**Table 4.** A study of the dynamics of modal analysis at 5 GHz for diametrically-fed dual port conducting body.

| Modal Dynamics | Modal Characteristics | Modal Inference |
|---|---|---|
| MS | High $Q$-Factor | Lower Bandwidth Potential |
| EV | $\lambda_n < 0$ | Capacitive Nature |
| CA | $\phi_n = 180°$ | At Resonance Condition |

The prototype of proposed antenna is fabricated by PCB prototyping, and $S$-parameters are measured by Agilent N5247A PNA-X vector network analyzer (VNA). The far-field pattern is measured in an anechoic chamber. There is a slight difference between the simulated outcomes and measured results. It happens in our case, due to the discrepancies caused by experimental tolerances (actually took place during the measurement of $S$ parameter and measurement of far-field parameters). The inaccuracy during the fabrication process is related to the soldering of SMA connector, which is one of the primary reasons. Then the validation is also performed for other different MIMO metrics [57–59] such as TARC, ECC, CCL, and MEG, as shown in Figures 32–37.

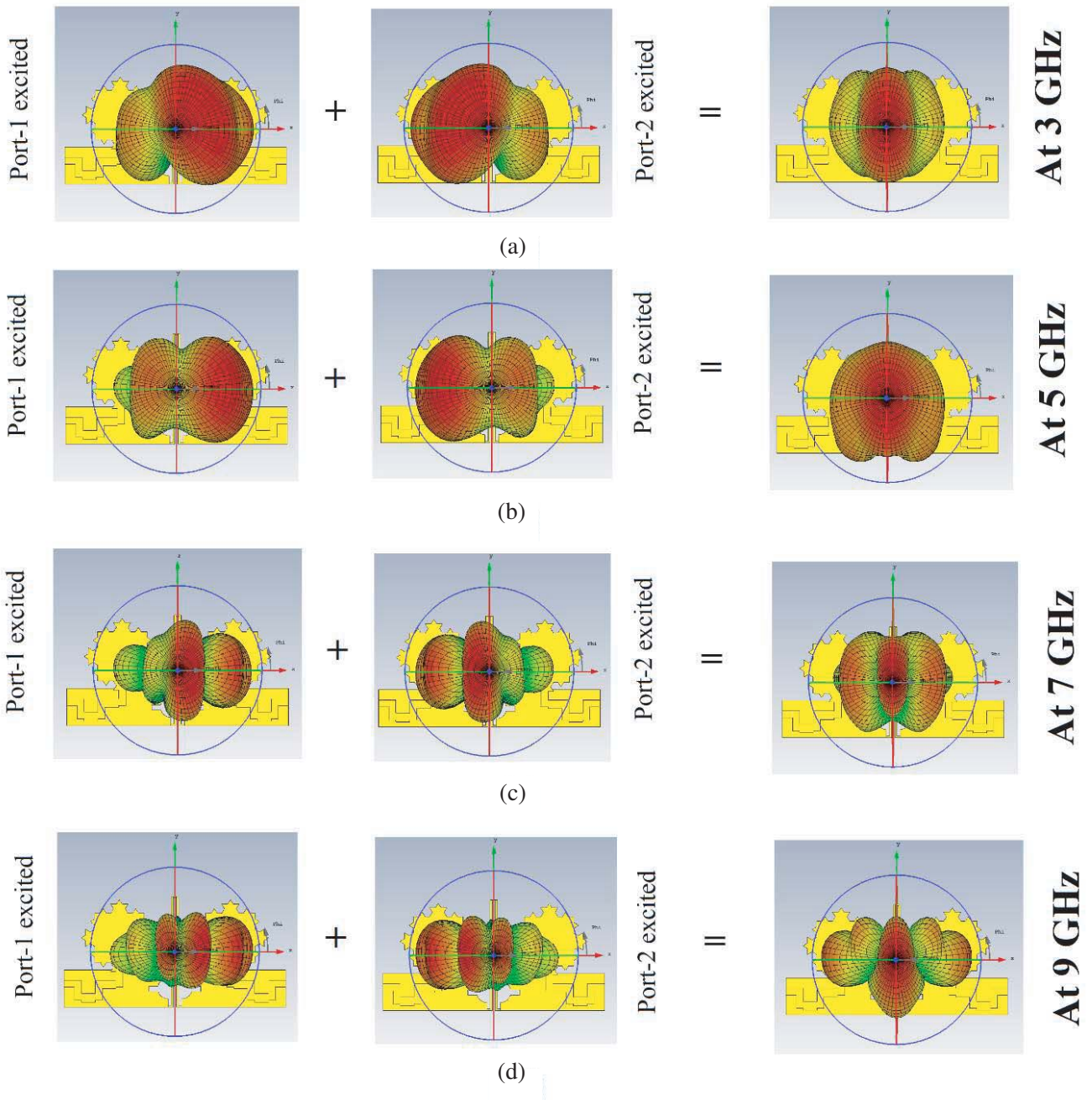


**Figure 28.** Modal radiation patterns at discrete frequencies.

**Table 5.** A study of the dynamics of modal analysis at 7 GHz for diametrically-fed dual port conducting body.

| Modal Dynamics | Modal Characteristics | Modal Inference |
|---|---|---|
| MS | Moderate $Q$-Factor | Moderate Bandwidth Potential |
| EV | $\lambda_n < 0$ | Capacitive Nature |
| CA | $\phi_n = 180^\circ$ | At Resonance Condition |

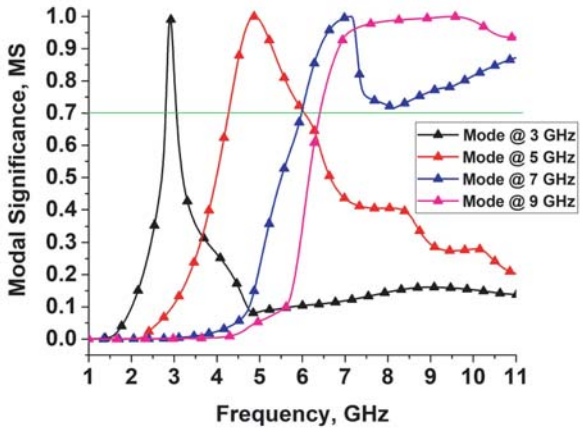


**Figure 29.** MS at discrete modal sweeps for diametrically-fed dual port conducting body.

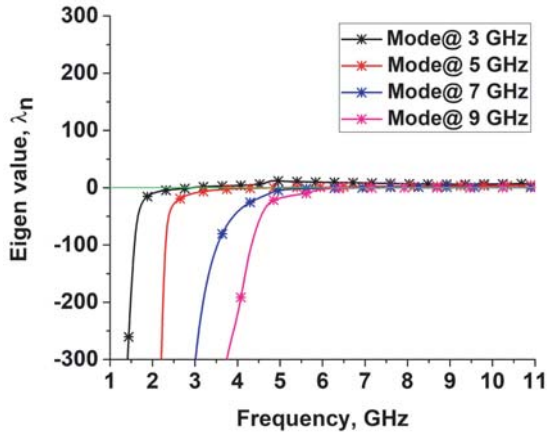


**Figure 30.** $\lambda_n$ at discrete modal sweeps for diametrically-fed dual port conducting body.

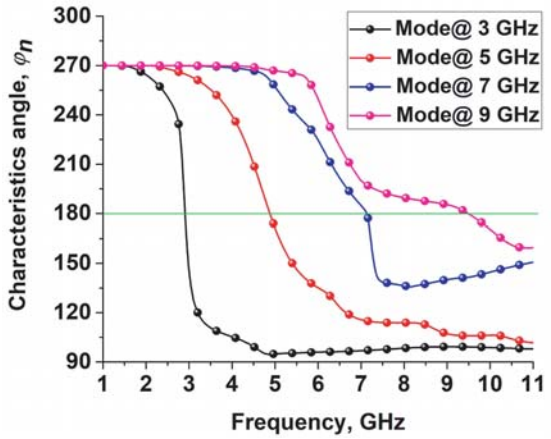


**Figure 31.** $\phi_n$ at discrete modal sweeps for diametrically-fed dual port conducting body.

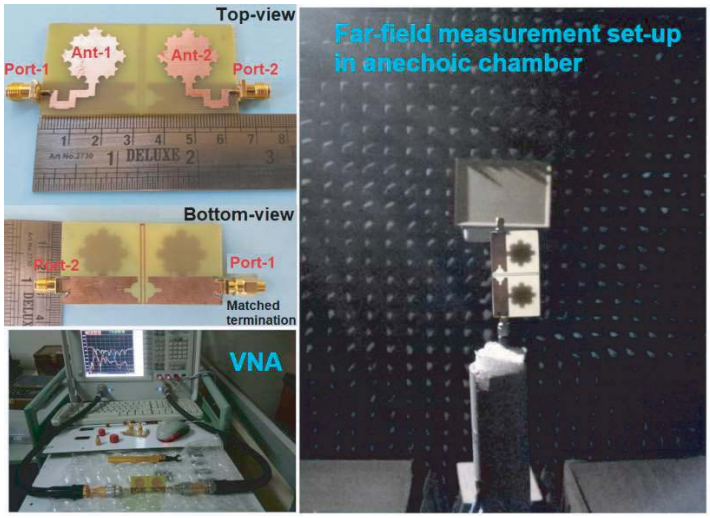


**Figure 32.** Fabricated prototype of the proposed diametrically-fed dual port fractal UWB MIMO antenna and its experimental setup present in the measurement lab for measuring various parameters.

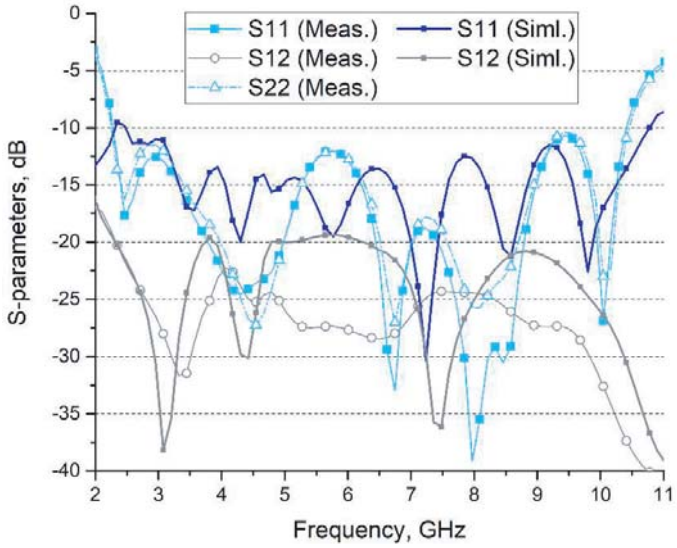


**Figure 33.** Simulated and measured $S$-parameters of diametrically-fed dual port fractal UWB MIMO antenna.

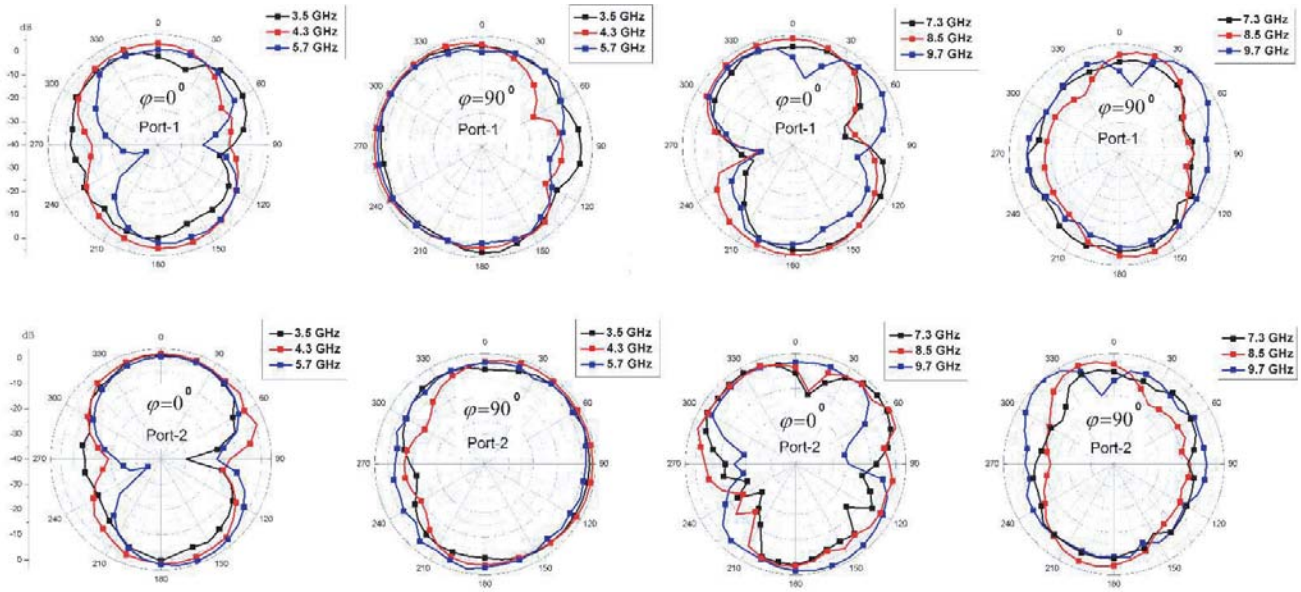


**Figure 34.** Measured radiation pattern of diametrically-fed dual port fractal UWB MIMO antenna.

**Table 6.** A study of the dynamics of modal analysis at 9 GHz for diametrically-fed dual port conducting body.

| Modal Dynamics | Modal Characteristics | Modal Inference |
|---|---|---|
| MS | Low $Q$-Factor | Wide Bandwidth Potential |
| EV | $\lambda_n < 0$ | Capacitive Nature |
| CA | $\phi_n = 180°$ | At Resonance Condition |

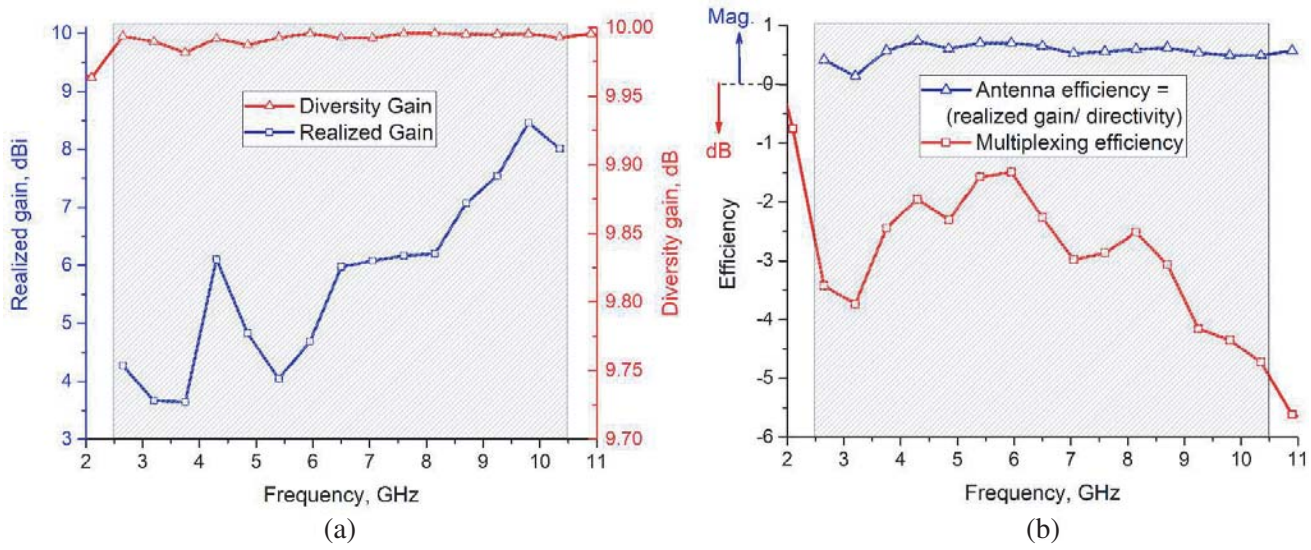


**Figure 35.** Measured realized gain and efficiency of diametrically-fed dual port fractal UWB MIMO antenna.

**Table 7.** Comparison of proposed UWB MIMO diversity antenna with other existing MIMO antennas [60–74].

| Ref. | Antenna geometry | $A_e$ ($\lambda^2$) | BW. | Isolation | GND | ECC | Peak Gain |
|---|---|---|---|---|---|---|---|
| 60 | Meandered Monopoles | 0.13 | 109.48% | > 15 dB | ■ | < 0.15 | —— |
| 61 | Bi-Planar Yagi-Like | 0.43 | 109.48% | > 17 dB | ■ | 0.0568 | 6 dBi |
| 62 | L-Shaped Slots | 0.11 | 44.8% | > 15 dB | ■ | 0.04 | 4.2 dBi |
| 63 | Circular Monopoles | 0.060 | 93.82% | > 22 dB | ■ | < 0.1 | 3.5 dBi |
| 64 | Coplanar Staircased Shaped | 0.122 | 115.06% | > 19 dB | □ | < 0.2 | 5.5 dBi |
| 65 | FSS Based Cuboid | 0.125 | 109.48% | ∼ 20 dB | □ | < 0.5 | —— |
| 66 | Quasi Self-Complementary | 0.033 | 133.93% | ∼ 20 dB | ■ | < 0.25 | 6.5 dBi |
| 67 | Stripline-Fed Staircased | 0.081 | 109.48% | ∼ 20 dB | □ | < 0.1 | 5.2 dBi |
| 68 | Microstrip + Stepped-Slot | 0.062 | 109.48% | > 18 dB | ■ | 0.004 | 3.8 dBi |
| 69 | (Circular + Square) Ring/2 | 0.041 | 111.42% | > 15 dB | □ | 0.1–0.2 | 3.5 dBi |
| 70 | Distinct PIFAs | 1.41 | 29% | > 15 dB | ■ | 0.08 | 3.39 dBi |
| 71 | P-Shaped Monopole | 0.06 | 131.03% | > 20 dB | ■ | 0.02 | 4.2 dBi |
| 72 | CPW + L-Shaped Element | 0.2 | 109.5% | > 14.2 dB | □ | 0.047 | 1.6 dBi |
| 73 | Patch + Parasitic Element | 0.607 | 13.7% | > 20 dB | □ | 0.05 | 5.8 dBi |
| 74 | Square Monopole + L-Slot | 0.056 | 118.2% | > 20 dB | □ | 0.004 | 3.32 dBi |
| Prop. | Fractal + Contorted Feed | 0.15 | 118.18% | > 22.5 dB | ■ | 0.025 | 8.4 dBi |

($A_e$) is the total electrical area; ($\lambda$) is calculated at lowest operating frequency, GND — Ground Plane; (■) denotes the connected ground; and (□) denotes the isolated ground.

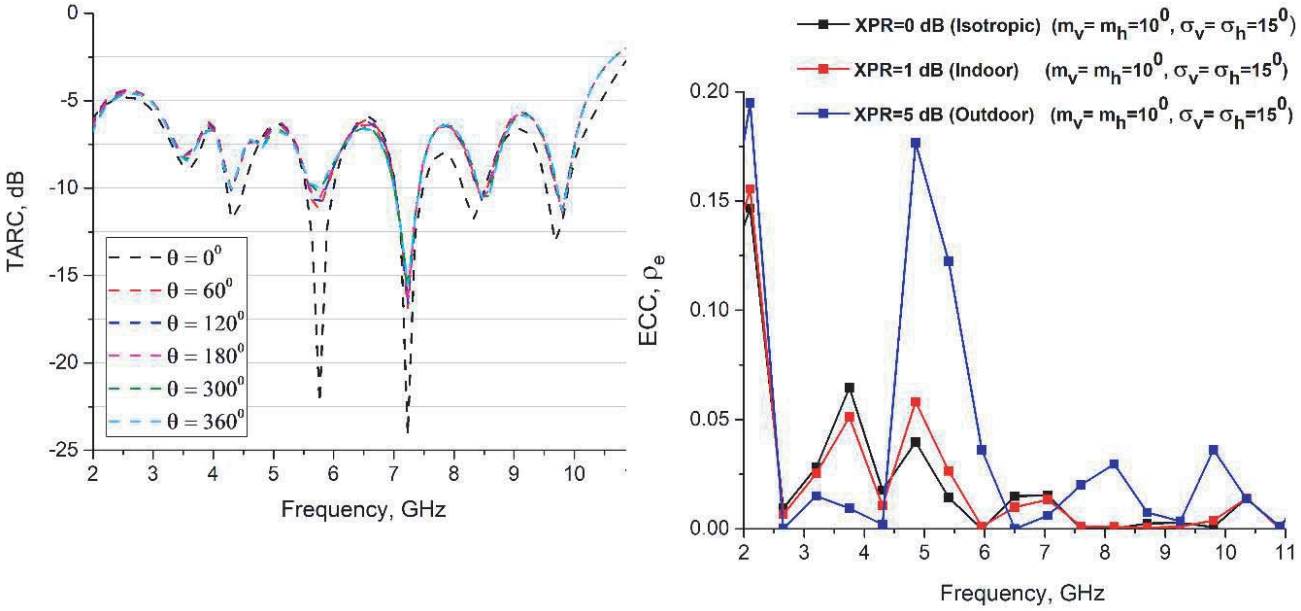


(a) (b)

**Figure 36.** (a) TARC (at different phase angles) and (b) ECC of proposed diametrically-fed dual port fractal UWB MIMO antenna.

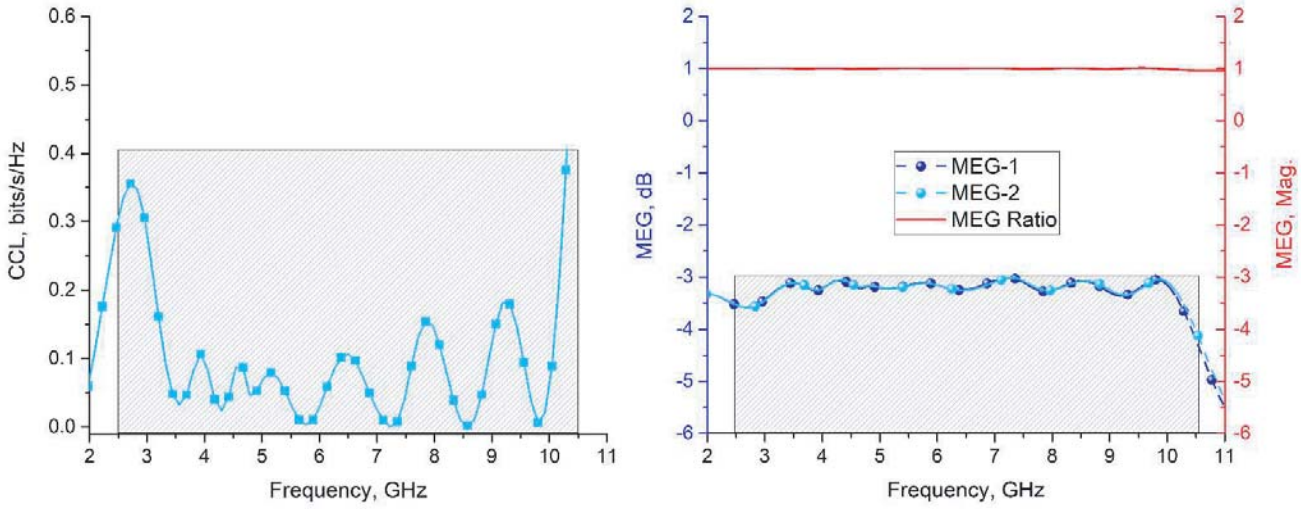


(a) (b)

**Figure 37.** (a) Channel Capacity Loss (CCL) and (b) Mean Effective Gain (MEG) of proposed diametrically-fed dual port fractal UWB MIMO antenna.

## 5. CONCLUSION

In this paper, the concept of classical approach inspired characteristics mode analysis (CMA) is reviewed from a theoretical viewpoint with reference to its recent trends, state-of-the-art developments, and its interpretation with a fractal UWB MIMO antenna. The physical insight provided by CMA enables a deterministic design approach, which is more efficient than lengthy optimization/trial-and-error process. It reveals intrinsic modal characteristics of the proposed conducting body. On a closer introspection, modal dynamics is performed on the ground of (a) modal significance (MS), (b) eigenvalues ($\lambda_n$), and

(c) characteristics angle ($\phi_n$) for different conducting bodies. Nevertheless, the modal surface current distributions and modal radiative patterns reveal the essential significant resonant modes along with the intrinsic nature of energy modes. The application of CMA in antenna structures is to decompose and synthesize surface currents or radiation fields. As the radiation field is decomposed into the superposition of orthogonal modes, the antenna performance is easier to optimize and can be realized from their physical principles.

Here, a 2-port UWB MIMO diversity antenna is designed, fabricated, and operates with measured bands from 2.4 to 10.4 GHz. The port isolations measures $> -22.5$ dB by introducing neutralization lines with slots. The design is investigated by CMA, which helps to improvise feeding configurations by analyzing characteristics modal parameters. The optimized design has a good impedance bandwidth of 118.18% and directive radiation patterns with peakgain of 8.4 dBi (can be extended for MIMO array applications). Calculated performance metrics seem excellent for MIMO pattern diversity applications. Simulated and measured validations show strong potentials of the proposed MIMO antenna, for the use in multi-disciplinary UWB multi-standard mobile/wireless/sensor ad-hoc diversity systems, which is proved through the comparative analysis with reported ones in [60–74], highlighted in Table 7. Besides progressive development in this area, there are still variety of rooms towards the achievement of tradeoffs, targeting contingent research outcomes for RF energy harvesting [75].

## 6. FUTURE WORKS AND OPEN CHALLENGES

In the present work, we have persuaded the modal analysis to establish physical insights (i.e., right from the geometrical features to performance deliverables and modal dynamics) about the proposed antenna model.

- For future works, we are currently trying to incorporate numerical modelling approach, as a utility for characteristics mode analysis (CMA), and would validate the MIMO performance characteristics.
- Insight on physical interpretation, numerical modelling, and CMA would be available in the same platform for more in-depth analysis.
- The future antenna designs can be modelled based on a parametric analysis, and CMA approach would be quite enough to track and resolve intrinsic performance complexities in compact and large antenna models.

## REFERENCES

1. Cabedo-Fabres, M., et al., "The theory of characteristic modes revisited: A contribution to the design of antennas for modern applications," *IEEE Antennas and Propagation Magazine*, Vol. 49, No. 5, 52–68, 2007.
2. Garbacz, R. J., "Modal expansions for resonance scattering phenomena," *Proceedings of the IEEE*, Vol. 53, No. 8, 856–864, 1965.
3. Garbacz, R. J., "A generalized expansion for radiated and scattered fields," Ph.D. dissertation, Ohio State University, Columbus, Ohio, USA, 1968.
4. Garbacz, R. J. and R. H. Turpin, "A generalized expansion for radiated and scattered fields," *IEEE Transactions on Antennas and Propagation*, Vol. 19, No. 3, 348–358, 1971.
5. Harrington, R. and J. Mautz, "The theory of characteristic modes for conducting bodies," *IEEE Transactions on Antennas and Propagation*, Vol. 19, No. 5, 622–628, 1971.
6. Harrington, R. and J. Mautz, "Computation of characteristic modes for conducting bodies," *IEEE Transactions on Antennas and Propagation*, Vol. 19, No. 5, 629–639, 1971.
7. Li, W., et al., "Modal proportion analysis in antenna characteristic mode theory," *International Journal of Antennas and Propagation*, Article ID 7069230, 10 Pages, 2019.
8. Vogel, M., et al., "Characteristic mode analysis: Putting physics back into simulation," *IEEE Antennas and Propagation Magazine*, Vol. 57, No. 2, 307–317, 2015.

9. Harrington, R., J. Mautz, and J. Y. Chang, "The theory of characteristic modes for dielectric and magnetic bodies," *IEEE Transactions and Antennas Propagation*, Vol. 20, No. 2, 194–198, 1972.
10. Martens, R. and D. Manteuffel, "Systematic design method of a mobile multiple antenna system using the theory of characteristic modes," *IET Microwaves, Antennas & Propagation*, Vol. 8, No. 12, 887–893, 2014.
11. Zhao, X., S. P. Yeo, and L. C. Ong, "Planar UWB MIMO antenna with pattern diversityand isolation improvement for mobile platform based on the theory of characteristic modes," *IEEE Transactions on Antennas and Propagation*, Vol. 66, No. 1, 420–425, 2017.
12. Singh, H. V. and S. Tripathi, "Compact UWB MIMO antenna with fork-shaped stub with Vias Based Coupling Current Steering (VBCCS) to Enhance Isolation Using CMA," *AEU — International Journal of Electronics and Communications*, Vol. 129, 153550, 2021.
13. Chen, Y. and C. F. Wang, "Electrically small UAV antenna design using characteristic modes," *IEEE Transactions on Antennas and Propagation*, Vol. 62, No. 2, 535–545, 2014.
14. Harrington, R. and J. Mautz, "Control of radar scattering by reactive loading," *IEEE Transactions on Antennas and Propagation*, Vol. 20, No. 4, 446–454, 1972.
15. Mautz, J. and R. Harrington, "Modal analysis of loaded $N$-port scatterers," *IEEE Transactions on Antennas and Propagation*, Vol. 21, No. 2, 188–199, 1973.
16. Harrington, R. and J. Mautz, "Pattern synthesis for loaded $N$-port scatterers," *IEEE Transactions on Antennas and Propagation*, Vol. 22, No. 2, 184–190, 1974.
17. Harrington, R. and J. Mautz, "Optimization of radar cross section of $N$-port loaded scatterers," *IEEE Transactions on Antennas and Propagation*, Vol. 22, No. 5, 697–701, 1974.
18. Wang, Y., et al., "Hybrid technique of fast RCS computation with characteristic modes and AWE," *IEEE Antennas and Wireless Propagation Letters*, Vol. 6, 464–467, 2007.
19. Li, H., Z. T. Miers, and B. K. Lau, "Design of orthogonal MIMO handset antennas based on characteristic mode manipulation at frequency bands below 1 GHz," *IEEE Transactions on Antennas and Propagation*, Vol. 62, No. 5, 2756–2766, 2014.
20. Li, H., et al., "Decoupling of multiple antennas in terminals with chassis excitation using polarization diversity, angle diversity and current control," *IEEE Transactions on Antennas and Propagation*, Vol. 60, No. 12, 5947–5957, 2012.
21. Kishor, K. K. and S. V. Hum, "A pattern reconfigurable chassis mode MIMO antenna," *IEEE Transactions on Antennas and Propagation*, Vol. 62, No. 6, 3290–3298, 2014.
22. Li, K. and Y. Shi, "Wideband MIMO handset antenna design based on theory of characteristic modes," *International Journal of RF and Microwave Computer-Aided Engineering*, Vol. 28, No. 4, e21217, 2018.
23. Raheja, D. K., B. K. Kanaujia, and S. Kumar, "Low profile four-port super-wideband multiple-input-multiple-output antenna with triple band rejection characteristics," *International Journal of RF and Microwave Computer-Aided Engineering*, Vol. 29, No. 10, e21831, 2019.
24. Li, Y., et al., "Metal-frame-integrated eight-element multiple-input multiple-output antenna array in the long term evolution bands 41/42/43 for fifth generation smartphones," *International Journal of RF and Microwave Computer-Aided Engineering*, Vol. 29, No. 1, e21495, 2019.
25. Sahu, N. K., G. Das, and R. K. Gangwar, "L-shaped dielectric resonator based circularly polarized Multi-Input-Multi-Output (MIMO) antenna for Wireless Local Area Network (WLAN) application," *International Journal of RF and Microwave Computer-Aided Engineering*, Vol. 28, No. 9, e21426, 2018.
26. Belazzoug, M. et al., "Ultra-compact 4-port DR antenna for multi-input multi-output standards," *International Journal of RF and Microwave Computer-Aided Engineering*, Vol. 30, No. 5, e22145, 2020.
27. Niu, B.-J. and J.-H. Tan, "Compact tri-band MIMO antenna based on quarter-mode slotted substrate-integrated-waveguide cavity," *International Journal of RF and Microwave Computer-Aided Engineering*, Vol. 30, No. 3, e22101, 2020.

28. Chattha, H. T., "Compact high isolation wideband 4G and 5G multi-input multi-output antenna system for handheld and internet of things applications," *International Journal of RF and Microwave Computer-Aided Engineering*, Vol. 29, No. 6, e21710, 2019.
29. Deng, J., J. Li, and L. Guo, "Decoupling of a three-port MIMO antenna with different impedances using reactively loaded dummy elements," *IEEE Antennas and Wireless Propagation Letters*, Vol. 17, No. 3, 430–433, 2018.
30. Raheja, D. K., et al., "Compact four-port MIMO antenna on slotted-edge substrate with dual-band rejection characteristics," *International Journal of RF and Microwave Computer-Aided Engineering*, Vol. 29, No. 7, e21756, 2019.
31. Singh, H. V. and S. Tripathi, "Compact UWB MIMO antenna with cross-shaped unconnected ground stub using characteristic mode analysis," *Microwave and Optical Technology Letters*, Vol. 61, No. 7, 1874–1881, 2019.
32. Srivastava, K., et al., "A CPW-fed UWB MIMO antenna with integrated GSM band and dual band notches," *International Journal of RF and Microwave Computer-Aided Engineering*, Vol. 29, No. 1, e21433, 2019.
33. Kumar, N. and R. Khanna, "A compact multi-band multi-input multi-output antenna for 4G/5G and IoT devices using theory of characteristic modes," *International Journal of RF and Microwave Computer-Aided Engineering*, Vol. 30, No. 1, e22012, 2020.
34. Malviya, L., M. V. Karthikeyan, and R. K. Panigrahi, "Multi-standard, multi-band planar multiple input multiple output antenna with diversity effects for wireless applications," *International Journal of RF and Microwave Computer-Aided Engineering*, Vol. 29, No. 2, e21551, 2019.
35. Biswas, A. K. and U. Chakraborty "A compact wide band textile MIMO antenna with very low mutual coupling for wearable applications," *International Journal of RF and Microwave Computer-Aided Engineering*, Vol. 29, No. 8, e21769, 2019.
36. Werner, D. H. and S. Ganguly, "An overview of fractal antenna engineering research," *IEEE Antennas and Propagation Magazine*, Vol. 45, No. 1, 38–57, 2003.
37. Rajkumar, S., et al., "A penta-band hybrid fractal MIMO antenna for ISM applications," *International Journal of RF and Microwave Computer-Aided Engineering*, Vol. 28, No. 2, e21185, 2017.
38. Gurjar, R., et al., "A novel compact self-similar fractal UWB MIMO antenna," *International Journal of RF and Microwave Computer-Aided Engineering*, Vol. 29, No. 3, e21632, 2018.
39. Mohanty, A. and S. Sahu, "High isolation two-port compact MIMO fractal antenna with Wi-MAX and X-band suppression characteristics," *International Journal of RF and Microwave Computer-Aided Engineering*, Vol. 30, No. 1, e22021, 2020.
40. Luo, Y., Z. N. Chen, and K. Ma, "Enhanced bandwidth and directivity of a dual-mode compressed high-order mode stub-loaded dipole using characteristic mode analysis," *IEEE Transactions on Antennas and Propagation*, Vol. 67, No. 3, 1922–1925, 2019.
41. Borchardt, J. J. and T. C. Lapointe, "U-slot patch antenna principle and design methodology using characteristic mode analysis and coupled mode theory," *IEEE Access*, Vol. 7, 109375–109385, 2019.
42. Luo, Y., Z. N. Chen, and K. Ma, "A single-layer dual-polarized differentially fed patch antenna with enhanced gain and bandwidth operating at dual compressed high-order modes using characteristic mode analysis," *IEEE Transactions on Antennas and Propagation*, Vol. 68, No. 5, 4082–4087, 2020.
43. Kim, D. and S. Nam, "Mutual coupling compensation in receive-mode antenna array based on characteristic mode analysis," *IEEE Transactions on Antennas and Propagation*, Vol. 66, No. 12, 7434–7438, 2018.
44. Dong, J., S. Wang, and J. Mo, "Design of a twelve-port MIMO antenna system for multi-mode 4G/5G smart-phone applications based on characteristic mode analysis," *IEEE Access*, Vol. 8, 90751–90759, 2020.
45. Wu, Q. and Z. Wen, "Time domain characteristic mode analysis for transmission problems," *IEEE Open Journal of Antennas and Propagation*, Vol. 1, 339–349, 2020.

46. Zhang, Z., X. Fu, and S. Cao, "Design of a vertically polarized patch antenna with switchable near-endfire beam using characteristic mode analysis," *IEEE Antennas and Wireless Propagation Letters*, Vol. 19, No. 7, 1157–1161, 2020.
47. Lin, F. H. and Z. N. Chen, "A method of suppressing higher order modes for improving radiation performance of metasurface multiport antennas using characteristic mode analysis," *IEEE Transactions on Antennas and Propagation*, Vol. 66, No. 4, 1894–1902, 2018.
48. Gao, G., et al., "Characteristic mode analysis of a nonuniform metasurface antenna for wearable applications," *IEEE Antennas and Wireless Propagation Letters*, Vol. 19, No. 8, 1355–1359, 2020.
49. Han, M. and W. Dou, "Compact clock-shaped broadband circularly polarized antenna based on characteristic mode analysis," *IEEE Access*, Vol. 7, 159952–159959, 2019.
50. Kim, D. and S. Nam, "Systematic design of a multiport MIMO antenna with bilateral symmetry based on characteristic mode analysis," *IEEE Transactions on Antennas and Propagation*, Vol. 66, No. 3, 1076–1085, 2018.
51. Mohanty, A. and B. R. Behera, "Investigation of 2-port UWB MIMO diversity antenna design using characteristics mode analysis," *AEU-International Journal of Electronics and Communications*, Vol. 124, 153–361, 2020.
52. Vandenbosch, G. A. E., "Reactive energies, impedance and Q factor of radiating structures," *IEEE Transactions on Antennas and Propagation*, Vol. 58, No. 4, 1112–1127, 2010.
53. Capek, M., et al., "The measurable $Q$ factor and observable energies of radiating structures," *IEEE Transactionson Antennas and Propagation*, Vol. 62, No. 1, 311–318, 2014.
54. Carpenter, C. J., "Electromagnetic energy and power in terms of charges and potentials instead of fields," *Proceedings of IEEE*, Vol. 136, No. 2, 55–65, 1989.
55. Capek, M., P. Hazdra, and J. Eichler, "A method for the evaluation of radiation Q based on modal approach," *IEEE Transactions on Antennas and Propagation*, Vol. 60, No. 10, 4556–4567, 2012.
56. Ghalib, A. and M. S. Sharawi, "New antenna mode generation based on theory of characteristic modes," *International Journal of RF and Microwave Computer-Aided Engineering*, Vol. 29, No. 6, e21686, 2019.
57. Naidu, P. R. T., et al., "Compact multiple EBG cells loaded UWB-narrowband antenna pair with high isolation for Cognitive Radio (CR) based MIMO applications," *AEU — International Journal of Electronics and Communications*, Vol. 127, 153420, 2020.
58. Reddy, T., R. Kumar, and R. K. Chaudhary, "Isolation enhancement and radar cross section reduction of MIMO antenna with frequency selective surface," *IEEE Transactions on Antennas and Propagation*, Vol. 66, No. 3, 1595–1600, 2018.
59. Alam, T., T. Reddy, and R. K. Chaudhary, "Integration of MIMO and cognitive radio for Sub-6 GHz 5G applications," *IEEE Antennas and Wireless Propagation Letters*, Vol. 18, No. 10, 2021–2025, 2019.
60. Deng, J.-Y., L.-X. Guo, and X.-L. Liu, "An ultrawideband MIMO antenna with a high isolation," *IEEE Antennas and Wireless Propagation Letters*, Vol. 15, 182–185, 2015.
61. Jehangir, S. S. and M. S. Sharawi, "A miniaturized UWB biplanar Yagi-like MIMO antenna system," *IEEE Antennas and Wireless Propagation Letters*, Vol. 16, 2320–2323, 2017.
62. Ren, J., et al., "Compact printed MIMO antenna for UWB applications," *IEEE Antennas and Wireless Propagation Letters*, Vol. 13, 1517–1520, 2014.
63. Zhang, S. and G. F. Pedersen, "Mutual coupling reduction for UWB MIMO antennas with wideband neutralization line," *IEEE Antennas and Wireless Propagation Letters*, Vol. 15, 166–169, 2015.
64. Roshna, T. K., U. Deepak, and P. Mohanan, "Compact UWB MIMO antenna for tridirectional pattern diversity characteristics," *IET Microwaves & Antennas Propagation*, Vol. 11, No. 14, 2059–2065, 2017.
65. Bilal, M., et al., "An FSS-based nonplanar quad-element UWB-MIMO antenna system," *IEEE Antennas and Wireless Propagation Letters*, Vol. 16, 987–990, 2016.

66. Liu, X.-L., et al., "A compact ultrawideband MIMO antenna using QSCA for high isolation," *IEEE Antennas and Wireless Propagation Letters*, Vol. 13, 1497–1500, 2014.
67. Roshna, T. K., et al., "A compact UWB MIMO antenna with reflector to enhance isolation," *IEEE Transactions and Antennas Propagation*, Vol. 63, No. 4, 1873–1877, 2015.
68. Luo, C.-M., J.-S. Hong, and L.-L. Zhong, "Isolation enhancement of a very compact UWB MIMO slot antenna with two defected ground structures," *IEEE Antennas and Wireless Propagation Letters*, Vol. 14, 1766–1769, 2015.
69. Alsath, M. G. N. and M. Kanagasabai, "Compact UWB monopole antenna for automotive communications," *IEEE Transactions on Antennas and Propagation*, Vol. 63, No. 9, 4204–4208, 2015.
70. Khan, R., et al., "Dual polarized antennas with reduced user effects for LTE-U MIMO mobile terminals," *AEU — International Journal of Electronics and Communications*, Vol. 111, 152880, 2019.
71. Nirmal, P. C., et al., "Compact wideband MIMO antenna for 4G Wi-MAX, WLAN and UWB applications," *AEU — International Journal of Electronics and Communications*, Vol. 99, 284–292, 2019.
72. Maurya, N. K. and R. Bhattacharya, "Design of compact dual-polarized multiband MIMOantenna using near-field for IoT," *AEU — International Journal of Electronics and Communications*, Vol. 117, 153091, 2020.
73. Tran, H. H., N. Hussain, and T. T. Le, "Low-profile wideband circularly polarized MIMO antenna with polarization diversity for WLAN applications," *AEU — International Journal of Electronics and Communications*, Vol. 108, 172–180, 2019.
74. Azarm, B., et al., "On development of a MIMO antenna for coupling reduction and Wi-MAX suppression purposes," *AEU — International Journal of Electronics and Communications*, Vol. 99, 226–235, 2019.
75. Behera, B. R., P. R. Meher, and S. K. Mishra, "Microwave antennas — An intrinsic part of RF energy harvesting systems: A contingent study about its design methodologies and state-of-art technologies in current scenario," *International Journal of RF and Microwave Computer-Aided Engineering*, Vol. 30, No. 5, e22148, 2020.